Multiple Higgs models and the 125 GeV state: an NMSSM perspective

Jack Gunion
U.C. Davis

36th Johns Hopkins Workshop, GGI, Oct. 16-19, 2012

Collaborators: G. Belanger, U. Ellwanger, Y. Jiang, S. Kraml, J. Schwarz

1. *"Higgs Bosons at 98 and 125 GeV at LEP and the LHC"* G. Belanger, U. Ellwanger, J. F. Gunion, Y. Jiang, S. Kraml and J. H. Schwarz. arXiv:1210.1976 [hep-ph]
2. *"Two Higgs Bosons at the Tevatron and the LHC?"* G. Belanger, U. Ellwanger, J. F. Gunion, Y. Jiang and S. Kraml. arXiv:1208.4952 [hep-ph]
3. *"Diagnosing Degenerate Higgs Bosons at 125 GeV"* J. F. Gunion, Y. Jiang and S. Kraml. arXiv:1208.1817 [hep-ph]
4. *"Could two NMSSM Higgs bosons be present near 125 GeV?"* J. F. Gunion, Y. Jiang and S. Kraml. arXiv:1207.1545 [hep-ph]
5. *"The Constrained NMSSM and Higgs near 125 GeV"* J. F. Gunion, Y. Jiang and S. Kraml. arXiv:1201.0982 [hep-ph] Phys. Lett. B **710**, 454 (2012)

Higgs-like LHC Excesses at 125 GeV

- **Experimental Higgs-like excesses: define**

$$R^h_Y(X) = \frac{\sigma(pp \to Y \to h)\mathrm{BR}(h \to X)}{\sigma(pp \to Y \to h_{SM})\mathrm{BR}(h_{SM} \to X)}\,, \quad R^h(X) = \sum_Y R^h_Y\,, \qquad (1)$$

where $Y = gg$ or WW.

Table 1: Summary of status for 125 GeV as of a few months ago — not important to get exact

$R(X)$, $X =$	$\gamma\gamma$	4ℓ	$\ell\nu\ell\nu$	$b\bar{b}$	$\tau^+\tau^-$
ATLAS	$\sim 1.9 \pm 0.5$	$\sim 1.1 \pm 0.6$	0.5 ± 0.6	0.5 ± 2.3	0.4 ± 2.0
CMS	$\sim 1.6 \pm 0.6$	$\sim 0.7 \pm 0.3$	0.6 ± 0.5	0.1 ± 0.7	$\sim 0 \pm 0.8$

In addition, we have

$$R^{\mathrm{ATLAS}}_{WW}(\gamma\gamma) = 2.5 \pm 1.2 \quad R^{\mathrm{CMS}}_{WW}(\gamma\gamma) = 2.3 \pm 1.3 \qquad (2)$$

and also there are CMS, ATLAS and D0+CDF=Tevatron measurements of Vh production with $h \to b\bar{b}$ giving at 125 GeV

$$R_{Vh}^{\rm CMS}(b\bar{b}) = 0.5 \pm 0.6\,, \quad R_{Vh}^{\rm ATLAS}(b\bar{b}) \sim 0.5 \pm 2.0\,, \quad R_{Vh}^{\rm Tev}(b\bar{b}) \sim 1.8 \pm 1\,, \tag{3}$$

all being very crude estimates.

Note: $R(WW) < 1$ would imply $gg \to h <$SM, but WW signal is diffuse and I will choose to mainly pay attention to $R(ZZ)$:

$R(ZZ) \gtrsim 1$ for ATLAS, whereas $R(ZZ) < 1$ for CMS.

- **The big questions:**

1. if the deviations from a single SM Higgs survive what is the model?
2. If they do survive, how far beyond our "standard" model set must we go to describe them?

Here, I focus on a a number of amusing possibilities in the NMSSM.

Enhanced Higgs signals in the NMSSM

- NMSSM=MSSM+$\widehat{S}$.
- The extra complex S component of $\widehat{S} \Rightarrow$ the NMSSM has h_1, h_2, h_2, a_1, a_2.
- The new NMSSM parameters of the superpotential (λ and κ) and scalar potential (A_λ and A_κ) appear as:

$$W \ni \lambda \widehat{S}\widehat{H}_u\widehat{H}_d + \frac{\kappa}{3}\widehat{S}^3\,, \quad V_{\rm soft} \ni \lambda A_\lambda S H_u H_d + \frac{\kappa}{3} A_\kappa S^3 \qquad (4)$$

- $\langle S\rangle \neq 0$ is generated by SUSY breakng and solves μ problem: $\mu_{\rm eff} = \lambda\langle S\rangle$.
- First question: Can the NMSSM give a Higgs mass as large as 125 GeV?

  Answer: Yes, so long as it is not a highly unified model. For our studies, we employed universal m_0, except for NUHM ($m^2_{H_u}$, $m^2_{H_d}$, m^2_S free), universal $A_t = A_b = A_\tau = A_0$ but allow A_λ and A_κ to vary freely. Of course, $\lambda > 0$ and κ are scanned demanding perturbativity up to the GUT scale.

- Can this model achieve rates in $\gamma\gamma$ and 4ℓ that are $>$SM?

  Answer: it depends on whether or not we insist on getting good a_μ.

- The possible mechanism (arXiv:1112.3548, Ellwanger) is to reduce the $b\bar{b}$ width of the mainly SM-like Higgs by giving it some singlet component. The gg and $\gamma\gamma$ couplings are less affected.

- Typically, this requires m_{h_1} and m_{h_2} to have similar masses (for singlet-doublet mixing) and large λ (to enhance Higgs mass).

  Large λ (by which we mean $\lambda > 0.1$) is only possible while retaining perturbativity up to m_{Pl} if $\tan\beta$ is modest in size.

  In the semi-unified model we employ, enhanced rates and/or large λ cannot be made consistent with decent δa_μ. (J. F. Gunion, Y. Jiang and S. Kraml.arXiv:1201.0982 [hep-ph])

- The "enhanced" SM-like Higgs can be either h_1 or h_2.

$$R_{gg}^{h_i}(X) \equiv (C_{gg}^{h_i})^2 \frac{\mathrm{BR}(h_i \to X)}{\mathrm{BR}(h_{SM} \to X)}, \quad R_{\mathrm{VBF}}^{h_i}(X) \equiv (C_{WW}^{h_i})^2 \frac{\mathrm{BR}(h_i \to X)}{\mathrm{BR}(h_{SM} \to X)}, \quad (5)$$

  where h_i is the i^{th} NMSSM scalar Higgs, and h_{SM} is the SM Higgs boson. The $C_Y^{h_i}$ is the ratio of the $Y \to h_i$ coupling relative to the $Y \to h_{SM}$ coupling.

Note that the corresponding ratio for $V^* \to V h_i$ $(V = W, Z)$ with $h_i \to X$ is equal to $R^{h_i}_{\rm VBF}(X)$ *in doublets + singlets models*.

Some illustrative R_{gg} results from (J. F. Gunion, Y. Jiang and S. Kraml. arXiv:1207.1545):

Figure Legend

	LEP/Teva	B-physics	$\Omega h^2 > 0$	$\delta a_\mu (\times 10^{10})$	XENON100	$R^{h_1/h_2}(\gamma\gamma)$
●	√	√	$0 - 0.136$	×	√	$[0.5, 1]$
■	√	√	$0 - 0.094$	×	√	$(1, 1.2]$
▲	√	√	$0 - 0.094$	×	√	> 1.2
■	√	√	0.094-0.136	×	√	$(1, 1.2]$
▲	√	√	0.094-0.136	×	√	> 1.2
♦	√	√	$0.094 - 0.136$	4.27-49.1	√	~ 1

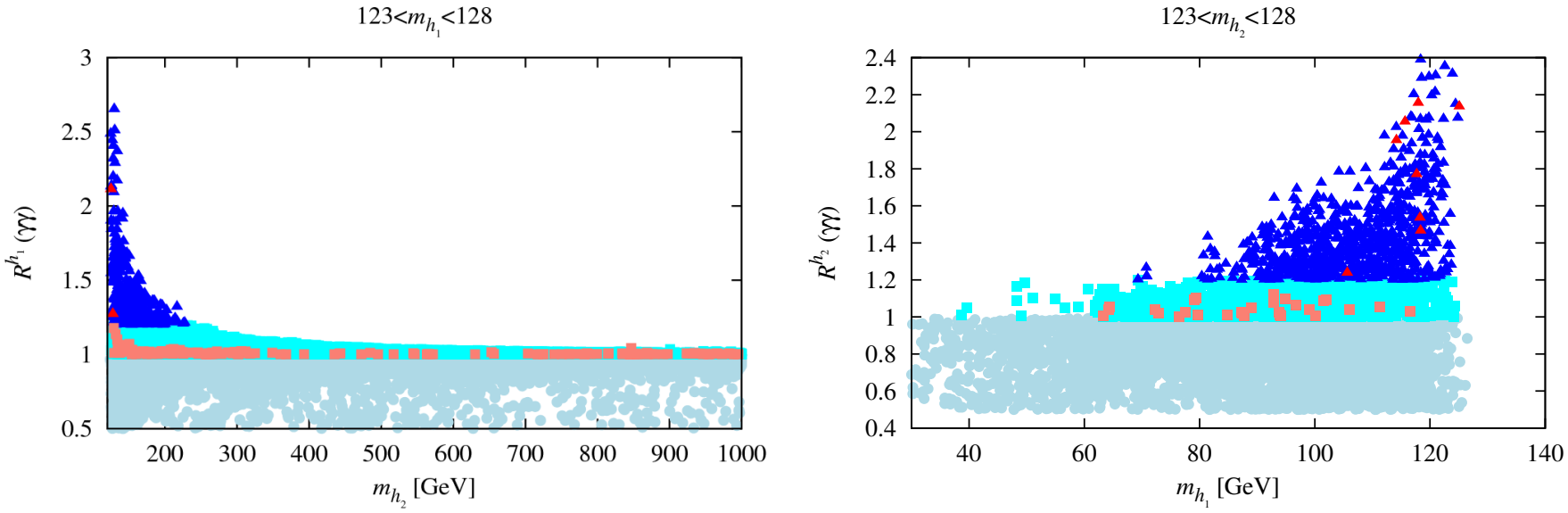

Figure 1: The plot shows $R_{gg}(\gamma\gamma)$ for the cases of $123 < m_{h_1} < 128$ GeV and $123 < m_{h_2} < 128$ GeV.

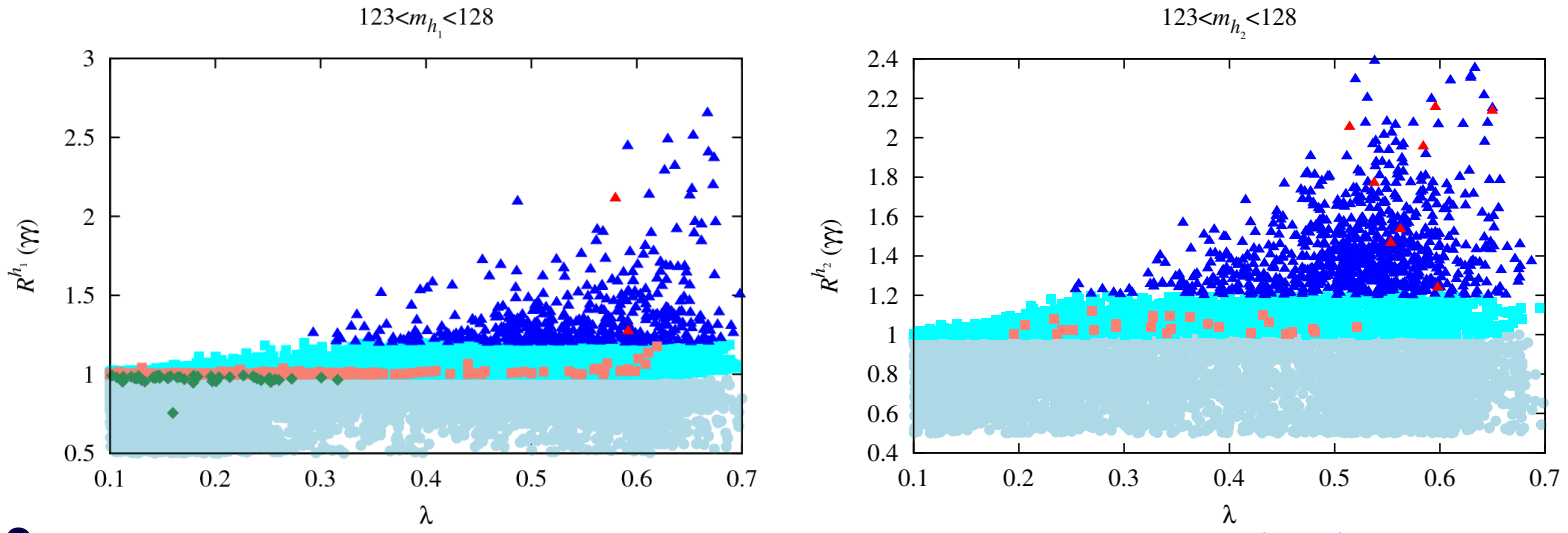

Figure 2: Observe the clear general increase in maximum $R_{gg}(\gamma\gamma)$ with increasing λ. Green points have good δa_μ, $m_{h_2} > 1$ TeV BUT $R_{gg}(\gamma\gamma) \sim 1$.

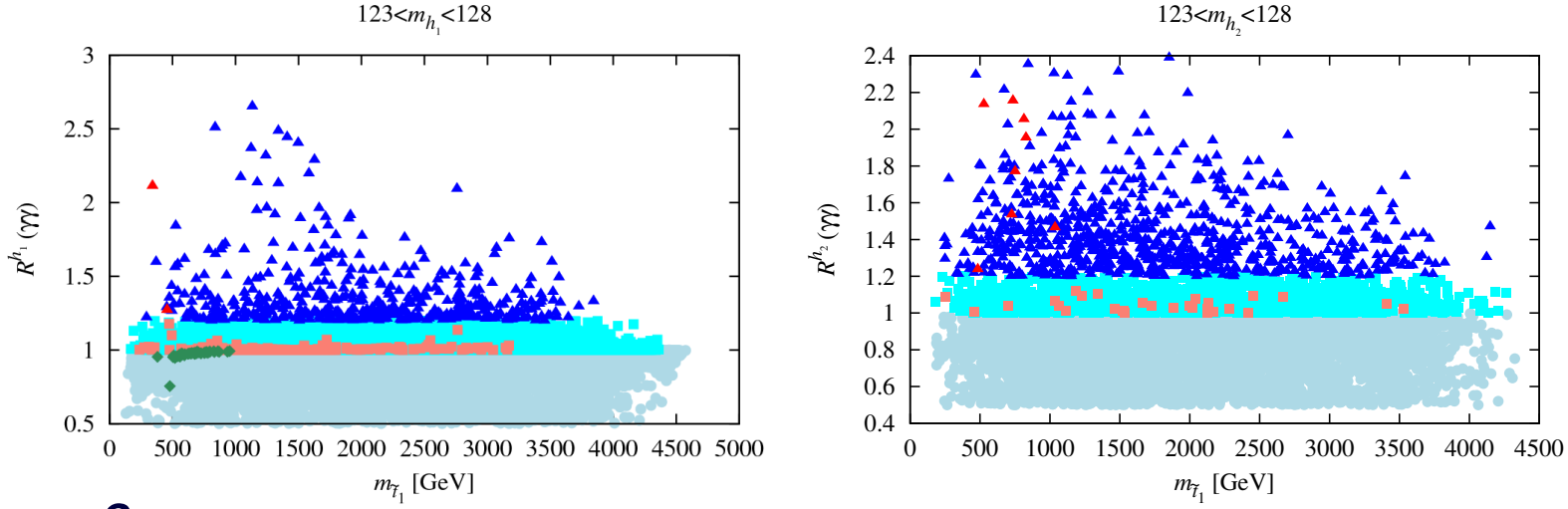

Figure 3: The lightest stop has mass $\sim 300 - 700$ GeV for red-triangle points.

- If we ignore δa_μ, then $R_{gg}(\gamma\gamma) > 1.2$ (even > 2) is possible while satisfying all other constraints provided h_1 and h_2 are close in mass, especially in the case where $m_{h_2} \in [123, 128]$ GeV window.

- This raises the issue of scenarios in which *both* m_{h_1} and m_{h_2} are in the $[123, 128]$ GeV window where the experiments see the Higgs signal.

- If h_1 and h_2 are sufficiently degenerate, the experimentalists might not have resolved the two distinct peaks, even in the $\gamma\gamma$ channel.

- The rates for the h_1 and h_2 could then add together to give an enhanced $\gamma\gamma$, for example, signal.

- The apparent width or shape of the $\gamma\gamma$ mass distribution could be altered.

- There is more room for an apparent mismatch between the $\gamma\gamma$ channel and other channels, such as $b\bar{b}$ or 4ℓ, than in non-degenerate situation.

  In particular, the h_1 and h_2 will generally have different gg and WW production rates and branching ratios.

Degenerate NMSSM Higgs Scenarios:

(arXiv:1207.1545, JFG, Jiang, Kraml)

- For the numerical analysis, we use NMSSMTools version 3.2.0, which has improved convergence of RGEs in the case of large Yukawa couplings.

- The precise constraints imposed are the following.

  1. Basic constraints: proper RGE solution, no Landau pole, neutralino LSP, Higgs and SUSY mass limits as implemented in NMSSMTools-3.2.0.
  2. B physics: $\mathrm{BR}(B_s \to X_s\gamma)$, ΔM_s, ΔM_d, $\mathrm{BR}(B_s \to \mu^+\mu^-)$, $\mathrm{BR}(B^+ \to \tau^+\nu_\tau)$ and $\mathrm{BR}(B \to X_s\mu^+\mu^-)$ at 2σ as encoded in NMSSMTools-3.2.0, plus updates.
  3. Dark Matter: $\Omega h^2 < 0.136$, thus allowing for scenarios in which the relic density arises at least in part from some other source.
     However, we single out points with $0.094 \leq \Omega h^2 \leq 0.136$, which is the 'WMAP window' defined in NMSSMTools-3.2.0.

4. 2011 XENON 100: spin-independent LSP–proton scattering cross section bounds implied by the neutralino-mass-dependent XENON100 bound. (For points with $\Omega h^2 < 0.094$, we rescale these bounds by a factor of $0.11/\Omega h^2$.) (2012 XENON 100 has little additional impact.)
5. δa_μ ignored: impossible to satisfy for scenarios we study here.

- Compute the effective Higgs mass in given production and final decay channels Y and X, respectively, and R^h_{gg} as

$$m_h^Y(X) \equiv \frac{R_Y^{h_1}(X) m_{h_1} + R_Y^{h_2}(X) m_{h_2}}{R_Y^{h_1}(X) + R_Y^{h_2}(X)} \qquad R_Y^h(X) = R_Y^{h_1}(X) + R_Y^{h_2}(X)\,. \tag{6}$$

- The extent to which it is appropriate to combine the rates from the h_1 and h_2 depends upon the degree of degeneracy and the experimental resolution.

  Very roughly, one should probably think of $\sigma_{\rm res} \sim 1.5$ GeV or larger. The widths of the h_1 and h_2 are very much smaller than this resolution.

- We perform scans covering the following parameter ranges:

$$0 \leq m_0 \leq 3000; \quad 100 \leq m_{1/2} \leq 3000; \quad 1 \leq \tan\beta \leq 40;$$
$$-6000 \leq A_0 \leq 6000; 0.1 \leq \lambda \leq 0.7; \quad 0.05 \leq \kappa \leq 0.5;$$
$$-1000 \leq A_\lambda \leq 1000; \quad -1000 \leq A_\kappa \leq 1000; \quad 100 \leq \mu_{eff} \leq 500\,. \qquad (7)$$

We only display points which pass the basic constraints, satisfy B-physics constraints, have $\Omega h^2 < 0.136$, obey the 2011 XENON100 limit on the LSP scattering cross-section off protons *and* have *both* h_1 and h_2 in the desired mass range: 123 GeV $< m_{h_1}, m_{h_2} < 128$ GeV.

- In Fig. 4, points are color coded according to $m_{h_2} - m_{h_1}$.

  Circular points have $\Omega h^2 < 0.094$, while diamond points have $0.094 \leq \Omega h^2 \leq 0.136$ (*i.e.* lie within the WMAP window).

- Many of the displayed points are such that $R^{h_1}_{gg}(\gamma\gamma) + R^{h_2}_{gg}(\gamma\gamma) > 1$.

- A few such points have Ωh^2 in the WMAP window.

  These points are such that either $R^{h_1}_{gg}(\gamma\gamma) > 2$ or $R^{h_2}_{gg}(\gamma\gamma) > 2$, with the R for the other Higgs being small. Scanning is continuing.

- **However, the majority of the points with $R_{gg}^{h_1}(\gamma\gamma) + R_{gg}^{h_2}(\gamma\gamma) > 1$ have $\Omega h^2 < 0.094$ and the $\gamma\gamma$ signal is often shared between the h_1 and the h_2.**

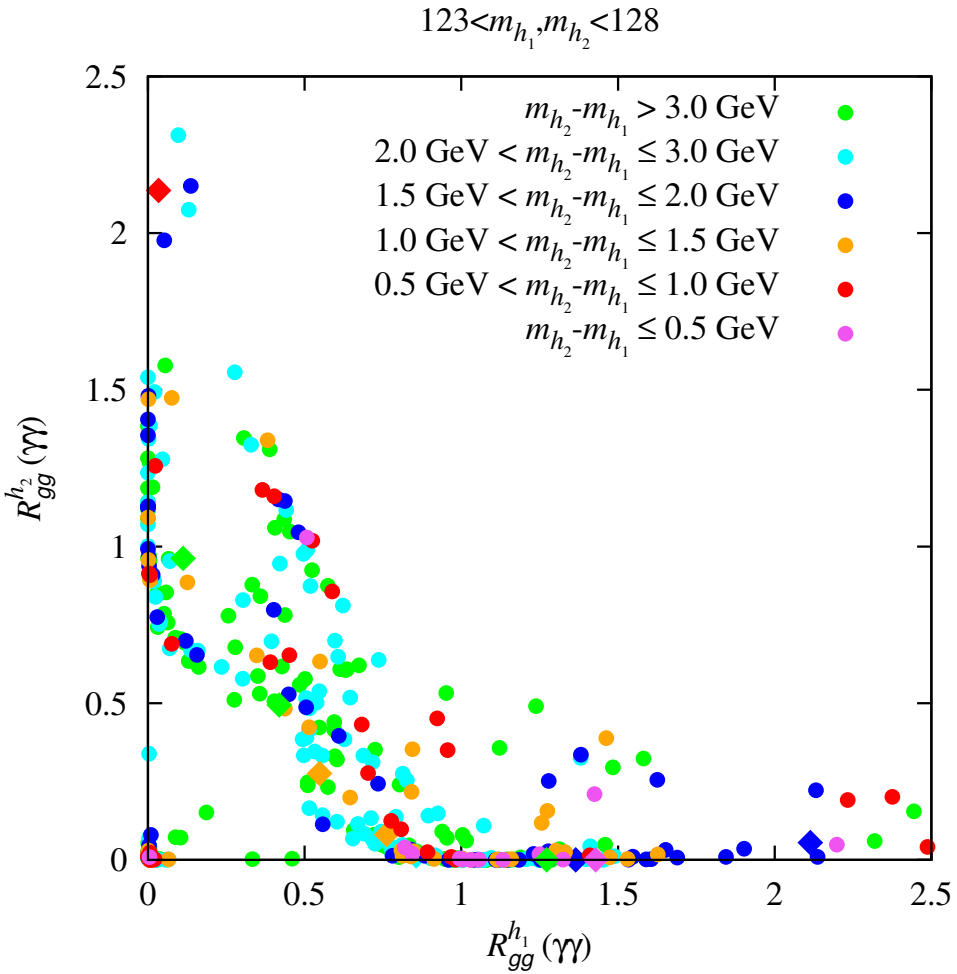

Figure 4: Correlation of $gg \to (h_1, h_2) \to \gamma\gamma$ signal strengths when both h_1 and h_2 lie in the 123–128 GeV mass range. The circular points have $\Omega h^2 < 0.094$, while diamond points have $0.094 \leq \Omega h^2 \leq 0.136$. Points are color coded according to $m_{h_2} - m_{h_1}$.

Now combine the h_1 and h_2 signals as described above. Recall: circular (diamond) points have $\Omega h^2 < 0.094$ ($0.094 \leq \Omega h^2 \leq 0.136$). Color code:

1. red for $m_{h_2} - m_{h_1} \leq 1$ GeV;
2. blue for 1 GeV $< m_{h_2} - m_{h_1} \leq 2$ GeV;
3. green for 2 GeV $< m_{h_2} - m_{h_1} \leq 3$ GeV.

- For current statistics and $\sigma_{\rm res} \gtrsim 1.5$ GeV we estimate that the h_1 and h_2 signals will not be seen separately for $m_{h_2} - m_{h_1} \leq 2$ GeV.

- In Fig. 5, we show results for $R^h_{gg}(X)$ for $X = \gamma\gamma, VV, b\bar{b}$. Enhanced $\gamma\gamma$ and VV rates from gluon fusion are very common.

- The bottom-right plot shows that enhancement in the Wh with $h \to b\bar{b}$ rate is also natural, though not as large as the best fit value suggested by the new Tevatron analysis.

- Diamond points (*i.e.* those in the WMAP window) are rare, but typically show enhanced rates.

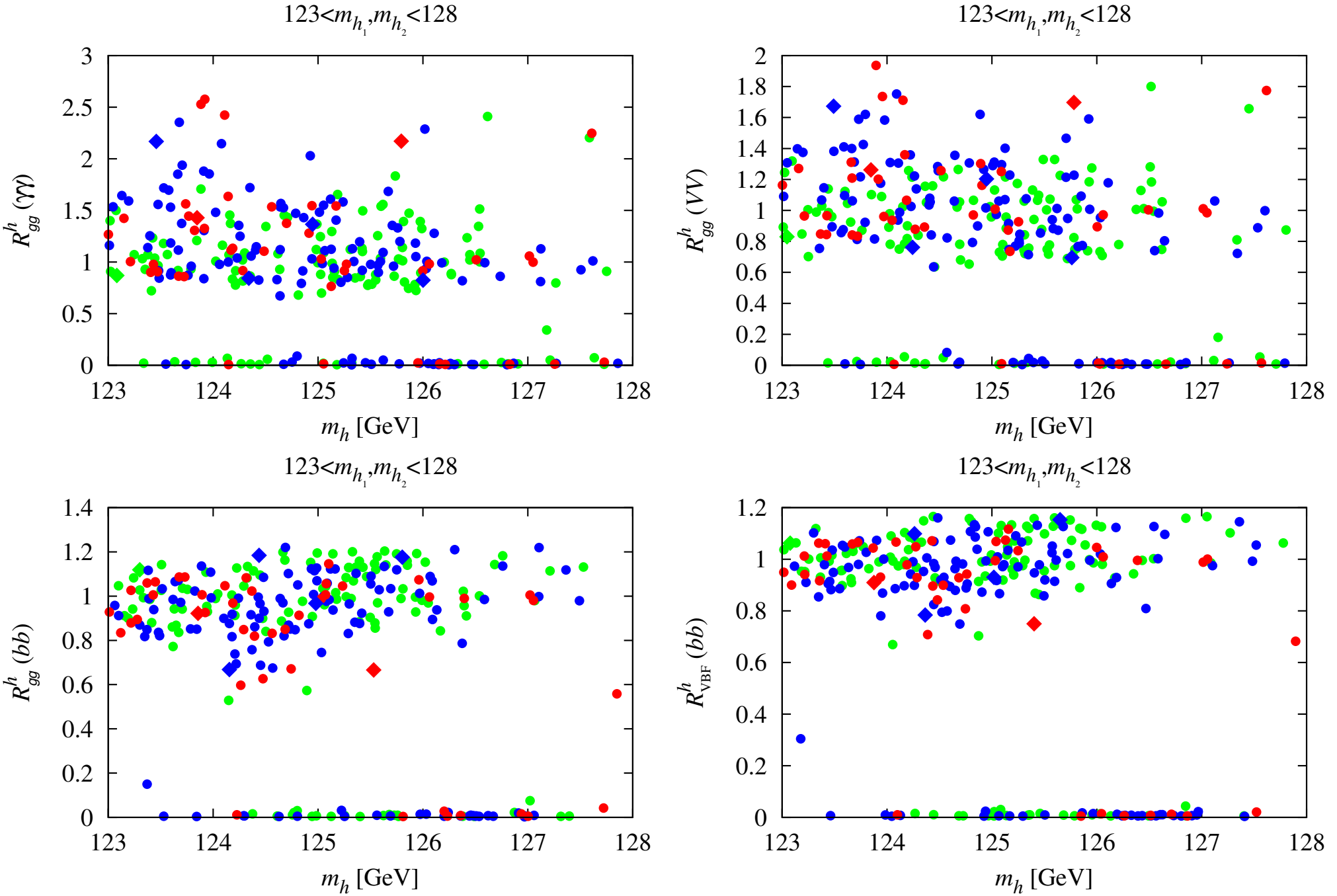

Figure 5: $R^h_{gg}(X)$ **for** $X = \gamma\gamma, VV, b\bar{b}$**, and** $R^h_{\rm VBF}(b\bar{b})$ **versus** m_h**. For application to the Tevatron, note that** $R^h_{\rm VBF}(b\bar{b}) = R^h_{W^*\to Wh}(b\bar{b})$**.**

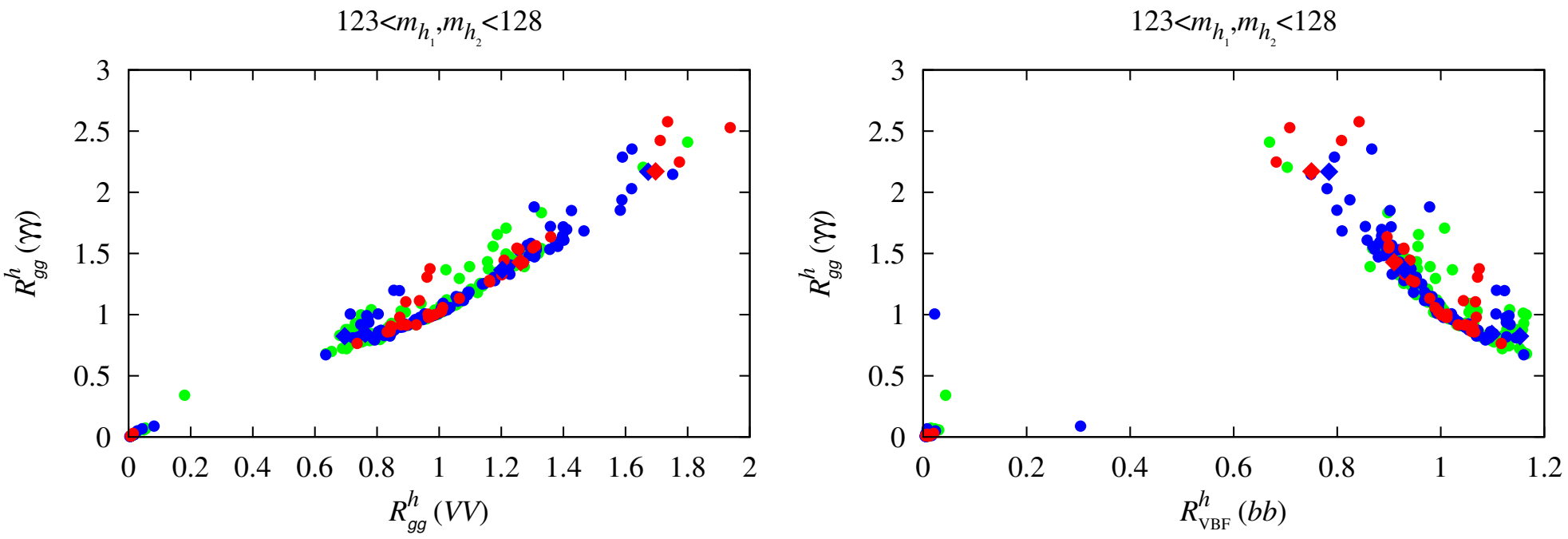

Figure 6: **Left: correlation between the gluon fusion induced $\gamma\gamma$ and VV rates relative to the SM. Right: correlation between the gluon fusion induced $\gamma\gamma$ rate and the WW fusion induced $b\bar{b}$ rates relative to the SM; the relative rate for $W^* \to Wh$ with $h \to b\bar{b}$ (relevant for the Tevatron) is equal to the latter.**

- **Comments on Fig. 6:**

  1. **Left-hand plot shows the strong correlation between $R^h_{gg}(\gamma\gamma)$ and $R^h_{gg}(VV)$.**

Note that if $R^h_{gg}(\gamma\gamma) \sim 1.5$, as suggested by current experimental results, then in this model $R^h_{gg}(VV) \geq 1.2$.

2. The right-hand plot shows the (anti) correlation between $R^h_{gg}(\gamma\gamma)$ and $R^h_{W^* \to Wh}(b\bar{b}) = R^h_{\rm VBF}(b\bar{b})$.
   In general, the larger $R^h_{gg}(\gamma\gamma)$ is, the smaller the value of $R^h_{W^* \to Wh}(b\bar{b})$.
   However, this latter plot shows that there *are* parameter choices for which both the $\gamma\gamma$ rate at the LHC and the $W^* \to Wh(\to b\bar{b})$ rate at the Tevatron (and LHC) can be enhanced relative to the SM as a result of there being contributions to these rates from both the h_1 and h_2.
3. It is often the case that one of the h_1 or h_2 dominates $R^h_{gg}(\gamma\gamma)$ while the other dominates $R^h_{W^* \to Wh}(b\bar{b})$. This is typical of the diamond WMAP-window points.
   However, a significant number of the circular $\Omega h^2 < 0.094$ points are such that either the $\gamma\gamma$ or the $b\bar{b}$ signal receives substantial contributions from both the h_1 and the h_2.
   We did not find points where the $\gamma\gamma$ and $b\bar{b}$ final states *both* receive substantial contributions from *both* the h_1 and h_2.

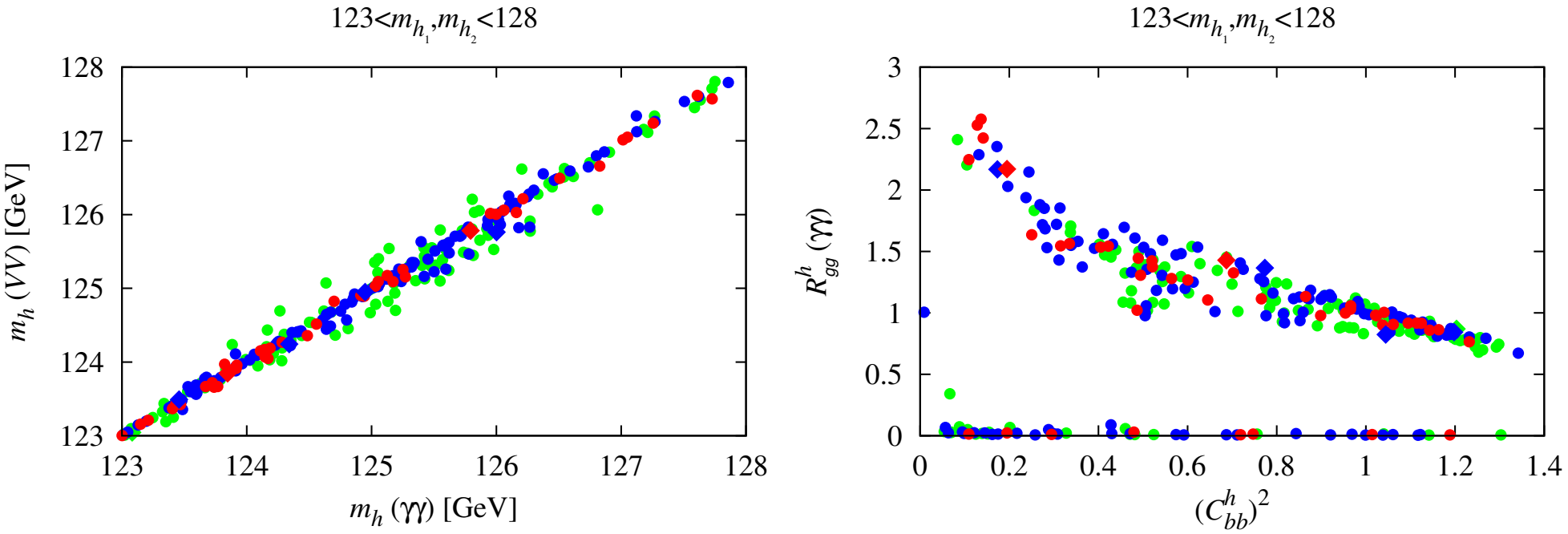

Figure 7: Left: effective Higgs masses obtained from different channels: $m_h^{gg}(\gamma\gamma)$ versus $m_h^{gg}(VV)$. Right: $\gamma\gamma$ signal strength $R^h_{gg}(\gamma\gamma)$ versus effective coupling to $b\bar{b}$ quarks $(C^h_{b\bar{b}})^2$. Here, $C^{h\ 2}_{b\bar{b}} \equiv \left[R^{h_1}_{gg}(\gamma\gamma)C^{h_1\ 2}_{b\bar{b}} + R^{h_2}_{gg}(\gamma\gamma)C^{h_2\ 2}_{b\bar{b}}\right] / \left[R^{h_1}_{gg}(\gamma\gamma) + R^{h_2}_{gg}(\gamma\gamma)\right]$.

Comments on Fig. 7

1. The m_h values for the gluon fusion induced $\gamma\gamma$ and VV cases are also strongly correlated — in fact, they differ by no more than a fraction of a

GeV and are most often much closer, see the left plot of Fig. 7.

2. The right plot of Fig. 7 illustrates the mechanism behind enhanced rates, namely that large net $\gamma\gamma$ branching ratio is achieved by reducing the average total width by reducing the average $b\bar{b}$ coupling strength.

- The dependence of $R^h_{gg}(\gamma\gamma)$ on λ, κ, $\tan\beta$ and $\mu_{\rm eff}$ is illustrated in Fig. 8.

  We observe that the largest $R^h_{gg}(\gamma\gamma)$ values arise at large λ, moderate κ, small $\tan\beta < 5$ (but note that $R^h_{gg}(\gamma\gamma) > 1.5$ is possible even for $\tan\beta = 15$) and small $\mu_{\rm eff} < 150$ GeV.

  Such low values of $\mu_{\rm eff}$ are very favorable in point of view of fine-tuning, in particular if stops are also light.

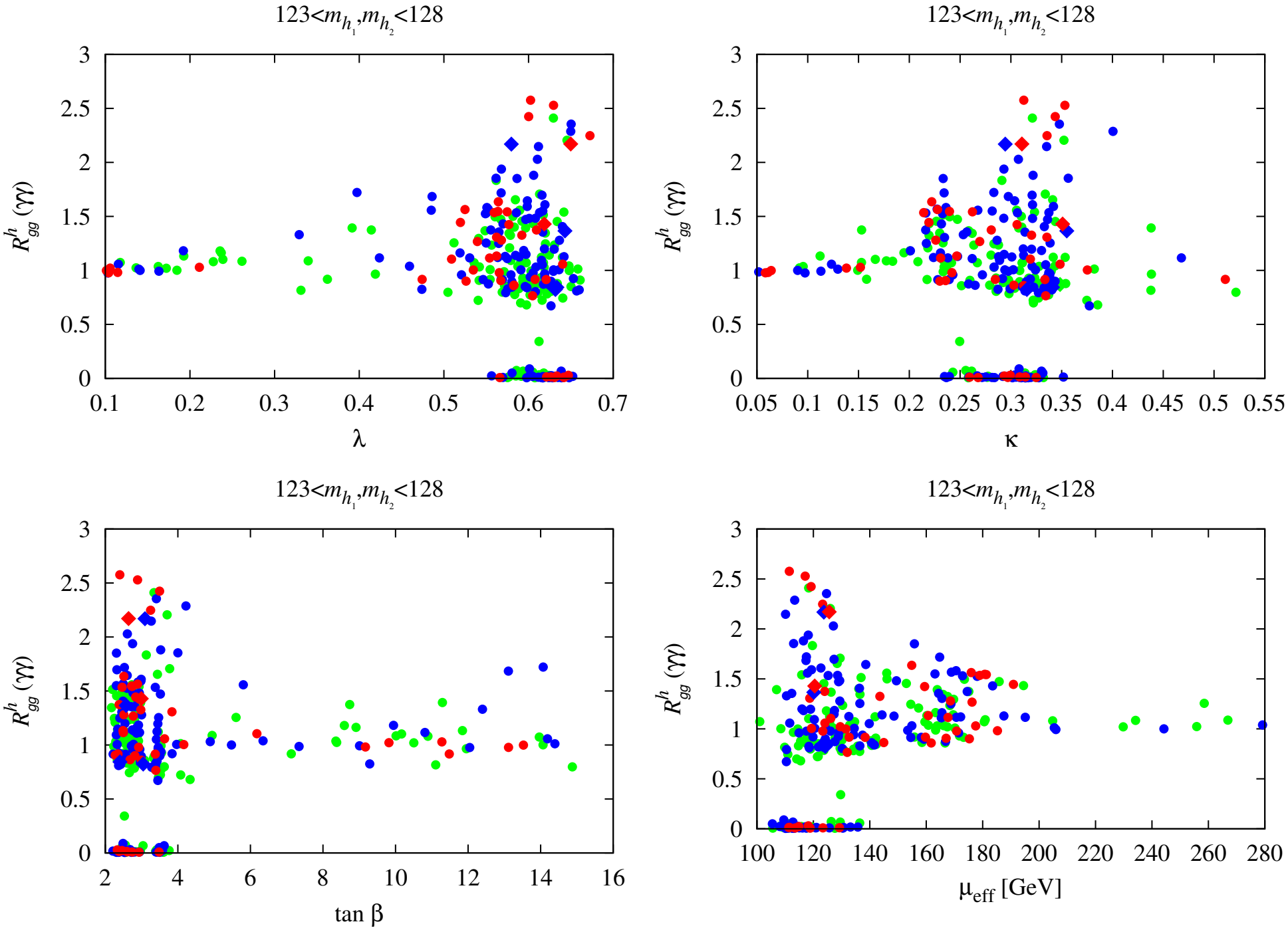

Figure 8: Dependence of $R^h_{gg}(\gamma\gamma)$ on λ, κ, $\tan\beta$ and $\mu_{\rm eff}$.

Fig. 9 shows that the stop mixing is typically large in these cases, $(A_t - \mu_{\rm eff}\cot\beta)/M_{\rm SUSY} \approx 1.5$–$2$. Moreover, the few points which we found in the WMAP window always have $m_{\tilde{t}_1} < 700$ GeV.

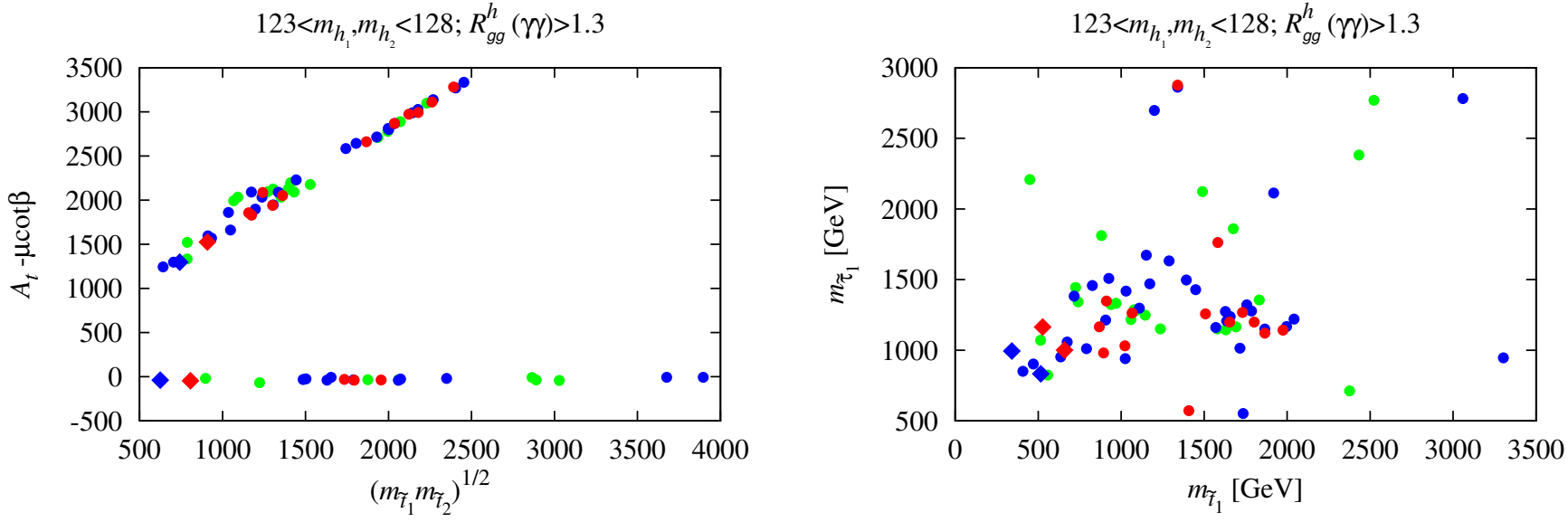

Figure 9: Left: Stop mixing parameter vs. $M_{\rm SUSY} \equiv \sqrt{m_{\tilde{t}_1} m_{\tilde{t}_2}}$. Right: $m_{\tilde{\tau}_1}$ vs. $m_{\tilde{t}_1}$. . Points plotted have $R^h_{gg}(\gamma\gamma) > 1.3$.

- Implications of the enhanced $\gamma\gamma$ rate scenarios for other observables are also quite interesting.

First, let us observe from Fig. 10 that these scenarios have squark and gluino masses that are above about 1.25 TeV ranging up to as high as 6 TeV (where our scanning more or less ended).

The WMAP-window points with large $R^h_{gg}(\gamma\gamma)$ are located at low masses of $m_{\tilde{g}} \sim 1.3$ TeV and $m_{\tilde{q}} \sim 1.6$ TeV.

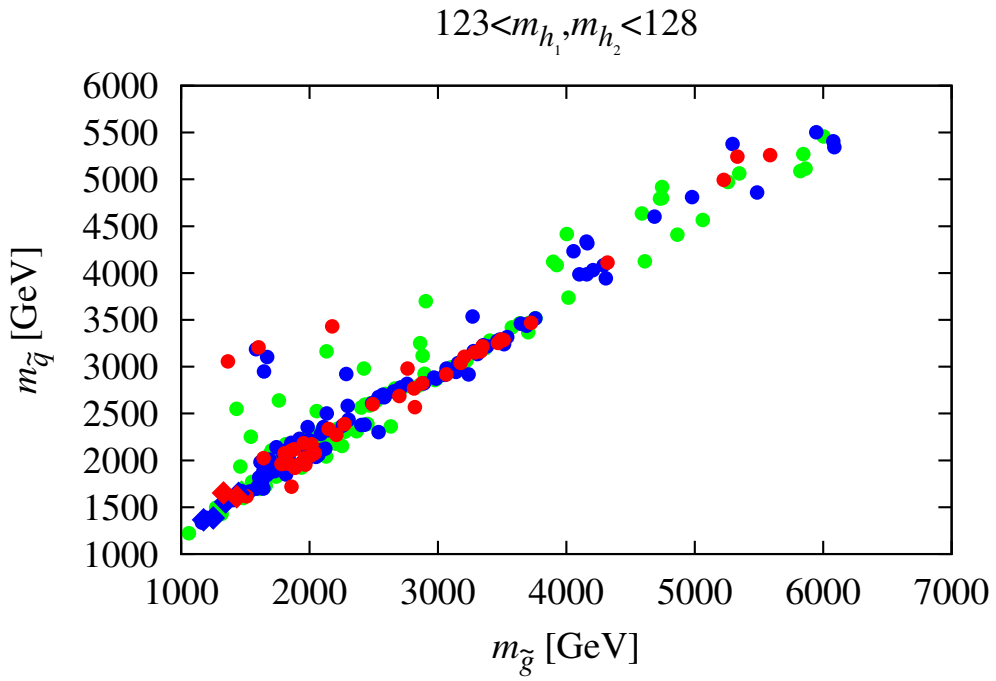

Figure 10: Average light-flavor squark mass, $m_{\tilde{q}}$, versus gluino mass, $m_{\tilde{g}}$, for the points plotted in the previous figures.

- **The value of $R^h_{gg}(\gamma\gamma)$ as a function of the masses of the other Higgs bosons is illustrated in Fig. 11.**

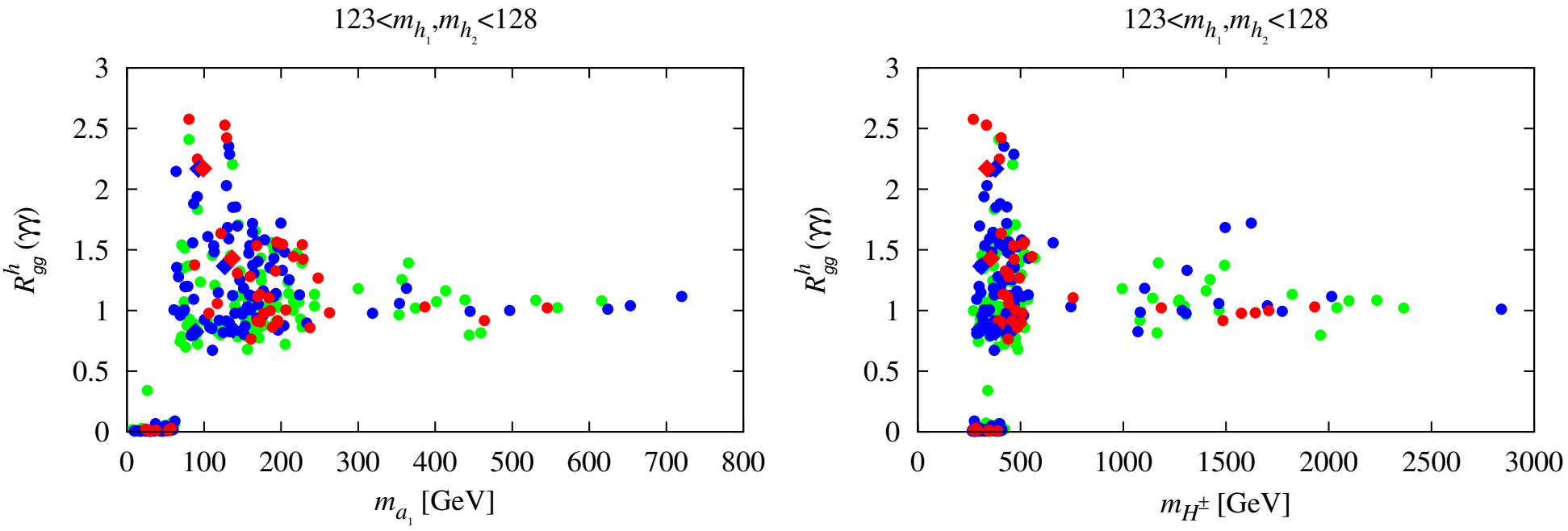

Figure 11: $R^h_{gg}(\gamma\gamma)$ versus the masses of m_{a_1} and $m_{H^\pm}$ (note that $m_{H^\pm} \simeq m_{a_2} \simeq m_{h_3}$).

Comments on Fig. 11:

1. **We see that values above of $R^h(\gamma\gamma) > 1.7$ are associated with masses**

for the a_2, h_3 and $H^\pm$ of order $\lesssim 500$ GeV and for the a_1 of order $\lesssim 150$ GeV.
(Note that $m_{a_2} \simeq m_{h_3} \simeq m_{H^\pm}$)
While modest in size, detectability of these states at such masses requires further study.

2. One interesting point is that $m_{a_1} \sim 125$ GeV is common for points with $R^h_{gg}(\gamma\gamma) > 1$ points.
We have checked that $R^{a_1}_{gg}(\gamma\gamma)$ is quite small for such points — typically $\lesssim 0.01$.

- In Fig. 12, we display Ωh^2 and the spin-independent cross section for LSP scattering on protons, σ_{SI}, for the points plotted in previous figures.

Comments on Fig. 12:

1. Very limited range of LSP masses consistent with the WMAP window, roughly $m_{\widetilde{\chi}^0_1} \in [60, 80]$ GeV.
2. Corresponding σ_{SI} values range from $few \times 10^{-9}$ pb to as low as $few \times 10^{-11}$ pb.

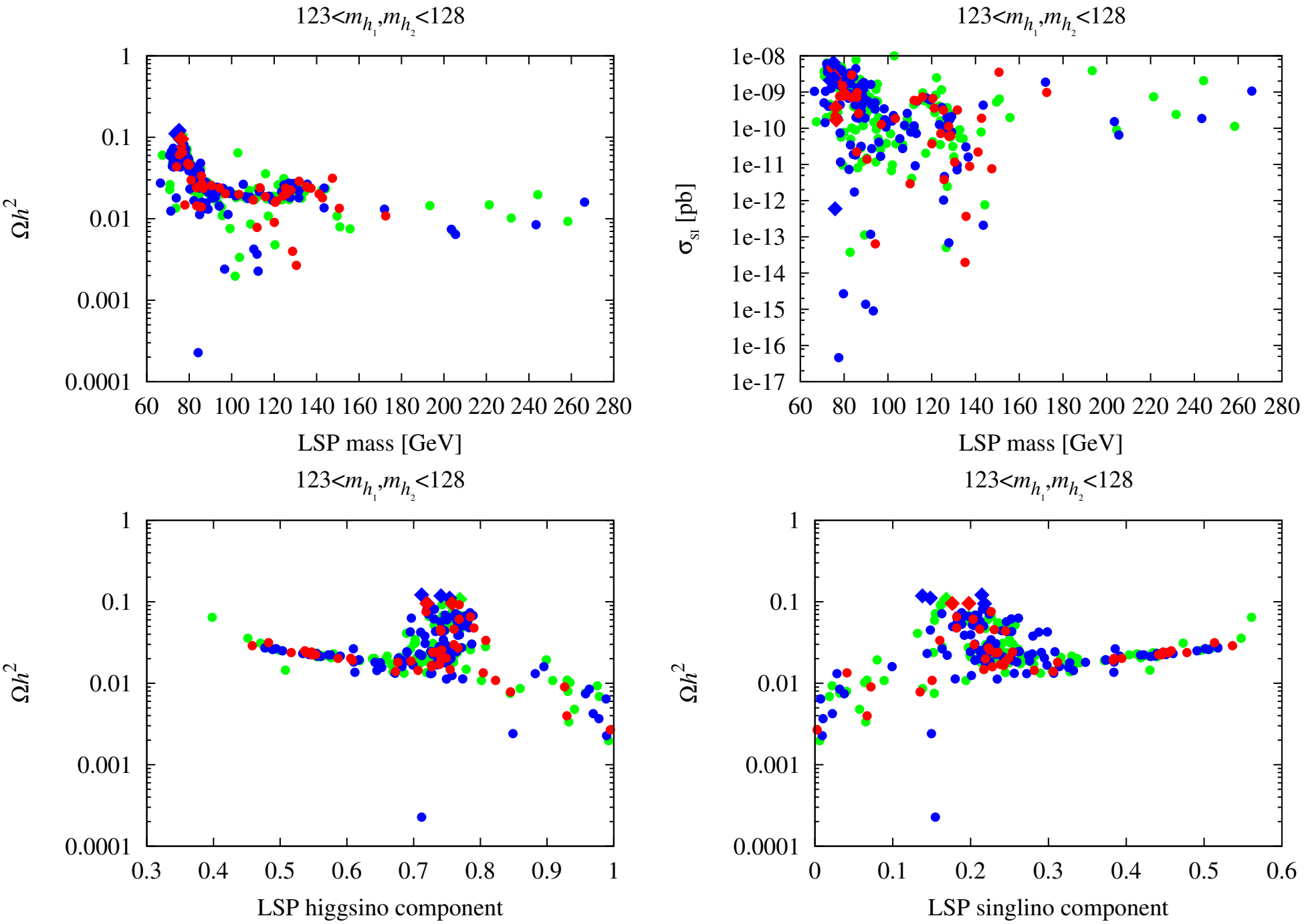

Figure 12: **Top row: Ωh^2 and spin-independent cross section on protons versus LSP mass for the points plotted in previous figures. Bottom row: Ωh^2 versus LSP higgsino (left) and singlino (right) components.**

3. Owing to the small $\mu_{\rm eff}$, the LSP is dominantly higgsino, which is also the reason for Ωh^2 typically being too low.
   The points with Ωh^2 within the WMAP window are mixed higgsino–singlino, with a singlino component of the order of 20%, see the bottom-row plots of Fig. 12.

- It is interesting to note a few points regarding the parameters associated with the points plotted in previous figures.

  1. For the WMAP-window diamond points, $\lambda \in [0.58, 0.65]$, $\kappa \in [0.28, 0.35]$, and $\tan\beta \in [2.5, 3.5]$.
  2. Points with $R^h_{gg}(\gamma\gamma) > 1.3$ have $\lambda \in [0.33, 0.67]$, $\kappa \in [0.22, 0.36]$, and $\tan\beta \in [2, 14]$.

- Can't find scenarios of this degenerate/enhanced type such that δa_μ is consistent with that needed to explain the current discrepancy.

  In particular, the very largest value of δa_μ achieved is of order 1.8×10^{-10} and, further, the WMAP-window points with large $R^h_{gg}(\gamma\gamma, VV)$ have $\delta a_\mu < 6 \times 10^{-11}$.

Diagnosing the presence of degenerate Higgses

(J. F. Gunion, Y. Jiang and S. Kraml. arXiv:1208.1817)

- Given that enhanced R^h_{gg} is very natural if there are degenerate Higgs mass eigenstates, how do we detect degeneracy? Must look at correlations among different R^h's.

- In the context of any doublets plus singlets model not all the R^{h_i}'s are independent; a complete independent set of R^h's can be taken to be:

$$R^h_{gg}(WW),\quad R^h_{gg}(bb),\quad R^h_{gg}(\gamma\gamma),\quad R^h_{VBF}(WW),\quad R^h_{VBF}(bb),\quad R^h_{VBF}(\gamma\gamma)\,. \tag{8}$$

Let us now look in more detail at a given $R^h_Y(X)$. It takes the form

$$R^h_Y(X) = \sum_{i=1,2} \frac{(C^{h_i}_Y)^2 (C^{h_i}_X)^2}{C^{h_i}_\Gamma} \tag{9}$$

where $C^{h_i}_X$ for $X = \gamma\gamma, WW, ZZ, \ldots$ is the ratio of the h_iX to $h_{SM}X$ coupling and $C^{h_i}_\Gamma$ is the ratio of the total width of the h_i to the SM Higgs

total width. The diagnostic tools that can reveal the existence of a second, quasi-degenerate (but non-interfering in the small width approximation) Higgs state are the double ratios:

$$\text{I):}\ \frac{R^h_{VBF}(\gamma\gamma)/R^h_{gg}(\gamma\gamma)}{R^h_{VBF}(bb)/R^h_{gg}(bb)},\quad \text{II):}\ \frac{R^h_{VBF}(\gamma\gamma)/R^h_{gg}(\gamma\gamma)}{R^h_{VBF}(WW)/R^h_{gg}(WW)},\quad \text{III):}\ \frac{R^h_{VBF}(WW)/R^h_{gg}(WW)}{R^h_{VBF}(bb)/R^h_{gg}(bb)}, \tag{10}$$

each of which should be unity if only a single Higgs boson is present but, due to the non-factorizing nature of the sum in Eq. (9), are generally expected to deviate from 1 if two (or more) Higgs bosons are contributing to the net h signals.

In a doublets+singlets model all other double ratios that are equal to unity for single Higgs exchange are not independent of the above three.

Of course, the above three double ratios are not all independent.

Which will be most useful depends upon the precision with which the R^h's for different initial/final states can be measured.

E.g measurements of R^h for the bb final state may continue to be somewhat imprecise and it is then double ratio II) that might prove most discriminating.

Or, it could be that one of the double ratios deviates from unity by a much larger amount than the others, in which case it might be most discriminating even if the R^h's involved are not measured with great precision.

- In Fig. 16, we plot the numerator versus the denominator of the double ratios I) and II), III) being very like I) due to the correlation between the $R^h_{gg}(\gamma\gamma)$ and $R^h_{gg}(WW)$ values discussed earlier.

- We observe that any one of these double ratios will often, but not always, deviate from unity (the diagonal dashed line in the figure).

- The probability of such deviation increases dramatically if we require (as apparently preferred by LHC data) $R^h_{gg}(\gamma\gamma) > 1$, see the solid (vs. open) symbols of Fig. 16.

  This is further elucidated in Fig. 17 where we display the double ratios I) and II) as functions of $R^h_{gg}(\gamma\gamma)$ (left plots).

  For the NMSSM, it seems that the double ratio I) provides the greatest discrimination between degenerate vs. non-degenerate scenarios with values

very substantially different from unity (the dashed line) for the majority of the degenerate NMSSM scenarios explored in the earlier section of this talk that have enhanced $\gamma\gamma$ rates.

Note in particular that I), being sensitive to the $b\bar{b}$ final state, singles out degenerate Higgs scenarios even when one or the other of h_1 or h_2 dominates the $gg \to \gamma\gamma$ rate, see the top right plot of Fig. 17.

In comparison, double ratio II) is most useful for scenarios with $R^h_{gg}(\gamma\gamma) \sim 1$, as illustrated by the bottom left plot of Fig. 17.

- Thus, as illustrated by the bottom right plot of Fig. 17, the greatest discriminating power is clearly obtained by measuring both double ratios.

In fact, a close examination reveals that there are no points for which *both* double ratios are exactly 1!

Of course, experimental errors may lead to a region containing a certain number of points in which both double ratios are merely consistent with 1 within the errors.

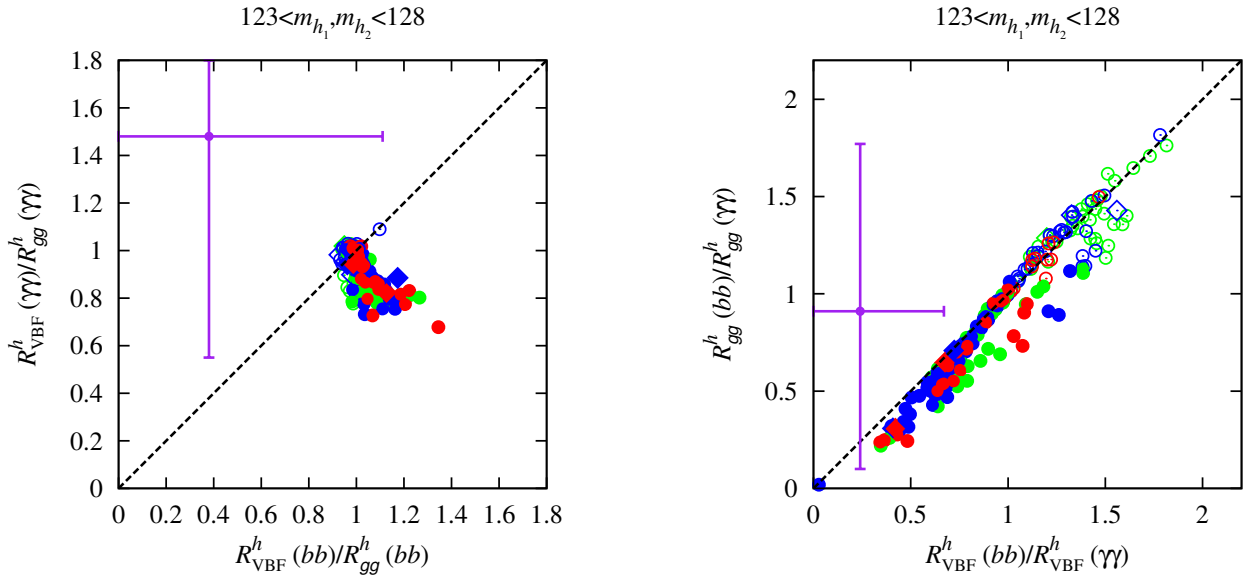

Figure 13: **Comparisons of pairs of event rate ratios that should be equal if only a single Higgs boson is present. The color code is green for points with $2\ \mathrm{GeV} < m_{h_2} - m_{h_1} \leq 3\ \mathrm{GeV}$, blue for $1\ \mathrm{GeV} < m_{h_2} - m_{h_1} \leq 2\ \mathrm{GeV}$, and red for $m_{h_2} - m_{h_1} \leq 1\ \mathrm{GeV}$. Large diamond points have Ωh^2 in the WMAP window of $[0.094, 0.136]$, while circular points have $\Omega h^2 < 0.094$. Solid points are those with $R^h_{gg}(\gamma\gamma) > 1$ and open symbols have $R^h_{gg}(\gamma\gamma) \leq 1$. Current experimental values for the ratios from CMS data along with their 1σ error bars are also shown.**

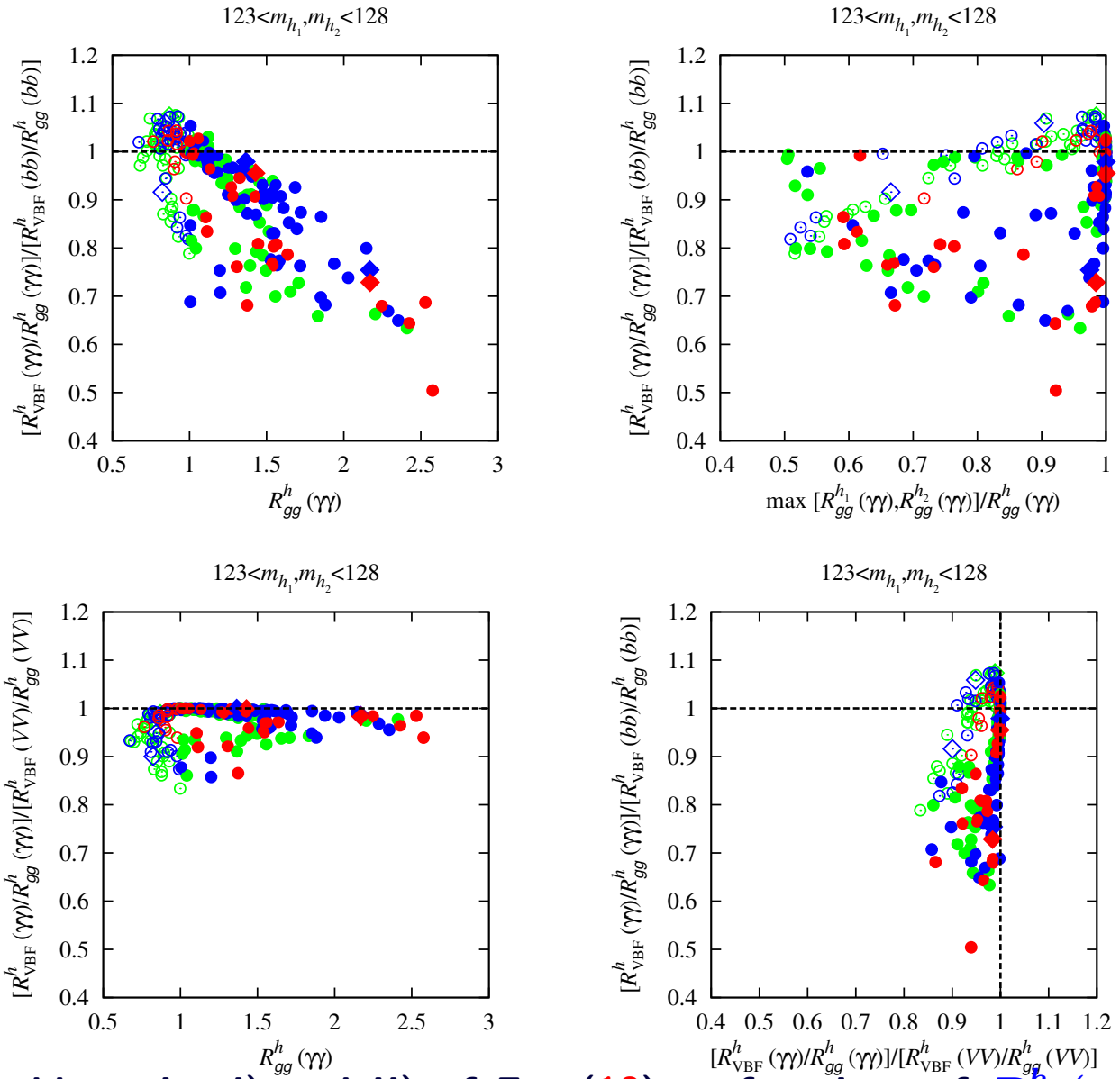

Figure 14: Double ratios I) and II) of Eq. (10) as functions of $R^h_{gg}(\gamma\gamma)$ (on the left). On the right we show (top) double ratio I) vs. $\max\left[R^{h_1}_{gg}(\gamma\gamma), R^{h_2}_{gg}(\gamma\gamma)\right]/R^h_{gg}(\gamma\gamma)$ and (bottom) double ratio I) vs. double ratio II) for the points displayed in Fig. 16. Colors and symbols are the same as in Fig. 16.

- **What does current LHC data say about these various double ratios?**

  The central values and 1σ error bars for the numerator and denominator of double ratios I) and II) obtained from CMS data [?] are also shown in Fig. 16.

  Obviously, current statistics are inadequate to discriminate whether or not the double ratios deviate from unity.

  About 100 times increased statistics will be needed. This will not be achieved until the $\sqrt{s} = 14$ TeV run with ≥ 100 fb^{-1} of accumulated luminosity.

  Nonetheless, it is clear that the double-ratio diagnostic tools will ultimately prove viable and perhaps crucial for determining if the ~ 125 GeV Higgs signal is really only due to a single Higgs-like resonance or if two resonances are contributing.

  Degeneracy has significant probability in model contexts if enhanced $\gamma\gamma$ rates are indeed confirmed at higher statistics.

Higgs at 125 GeV for LHC and 136 GeV for the Tevatron (and LHC?):

(G. Belanger, U. Ellwanger, J. F. Gunion, Y. Jiang and S. Kraml. arXiv:1208.4952)

1) A Higgs boson H_1 at 125–126 GeV

- Combining ATLAS and CMS:

$$R_1^{\gamma\gamma}(ggF) \simeq 1.66 \pm 0.36\,. \tag{11}$$

At CMS, combining the 7 TeV dijet tag and 8 TeV dijet tight results, yields $R_1^{\gamma\gamma}(VBF) \sim 2.6 \pm 1.3$; note that here the VBF category contains roughly 25% ggF production.

For ATLAS, we obtain $R_1^{\gamma\gamma}(VBF) \sim 2.7 \pm 1.5$ (with unspecified ggF contamination).

Subsequently we merely assume $R_1^{\gamma\gamma}(VBF) > 1$.

- The ggF process also dominates the Higgs signal in the ZZ channel. The best fits to $R_1^{ZZ^{(*)}}(ggF)$ from the ATLAS and CMS collaborations are both consistent with 1: $R_1^{ZZ^{(*)}}(ggF) \simeq 1.4 \pm 0.6$ (ATLAS), $R_1^{ZZ^{(*)}}(ggF) \simeq 0.75 \pm 0.5$ (CMS).

  Combining, we estimate

$$R_1^{ZZ^{(*)}}(ggF) \simeq 1.02 \pm 0.38\,. \tag{12}$$

2) A Higgs boson H_2 at 135–136 GeV

- In the $\gamma\gamma$ mode, CMS has observed an excess of events of about two standard deviations around 136 GeV, the excess being a bit larger for the 7 TeV data than for the 8 TeV data.

  Combining the two data sets, the corresponding reduced signal rate can be estimated as $R_2^{\gamma\gamma}(ggF) \simeq 0.9 \pm 0.4$ (CMS).

  However, no excess of events at this mass was observed by ATLAS.

We estimate $R_2^{\gamma\gamma}(ggF) \simeq 0.0 + 0.4$ (ATLAS).

Taken together, one obtains

$$R_2^{\gamma\gamma}(ggF) \simeq 0.45 \pm 0.3\,. \tag{13}$$

The above is a crude estimate, which could be improved by more detailed analyses and/or more data; here we consider it as a first hint for the existence of a second state near 136 GeV in the Higgs sector.

- In the $ZZ^{(*)}$ mode, no excess has been observed by the ATLAS and CMS collaborations for $M_H \sim 136$ GeV.

  Combining both upper bounds on the reduced signal rate, we estimate

$$R_2^{ZZ^{(*)}}(ggF) \lesssim 0.2 \tag{14}$$

  at the level of one standard deviation.

3) Low mass resolution channels.

- In the $\tau\tau$ channel and tagging two jets (sensitive mostly to the VBF production mode), CMS observes a deficit with respect to the background-only hypothesis assuming $M_H \sim 125$ GeV.

  Hence $R_1^{\tau\tau}(VBF)$ should be as small as possible.

- Assuming $M_H \gtrsim 132$ GeV, CMS observes an excess of events of about half a standard deviation; the upper limit (for $M_{H_2} \sim 135$ GeV) is given as

$$R_2^{\tau\tau}(VBF) < 1.81\,. \tag{15}$$

  In the presence of two Higgs states these values have to be reinterpreted to account for overlapping signals — will not give details.

- In the bb channel, the CDF and D0 collaborations at the Tevatron (where the dominant production mode is VH) have observed large values of $R^{bb}(VH)$: $R_{125}^{bb}(VH) \simeq 1.97 + 0.74 - 0.68$ assuming $M_{H_{\rm SM}} = 125$ GeV, and

$$R_{135}^{bb}(VH) \simeq 3.53 + 1.26 - 1.16 \tag{16}$$

assuming $M_{H_{\rm SM}} = 135$ GeV.

CMS has also observed excesses in this channel, but below the expectations for a SM Higgs boson at 125 GeV.

Assuming larger values of $M_{H_{\rm SM}}$, the excesses observed by CMS are larger (with a peak around $M_{H_{\rm SM}} \sim 130$ GeV), but have large error bars.

It is clear that the central value of (16) is difficult to explain: the VH production cross section $\propto c_V^2$ cannot be enhanced with respect to the SM, and the SM Higgs branching fraction of $\sim 40\%$ for $M_{H_{\rm SM}} = 135$ GeV can be enhanced at most by a factor of 2.5 in the unphysical limit $c_D \to \infty$.

- Using the same reduced couplings for Higgs bosons to b-quarks and τ-leptons, one finds

$$R^{bb}(VH) = R^{\tau\tau}(VBF) \tag{17}$$

for all Higgs states.

If $R_1^{\tau\tau}(VBF)$ is as small as observed by CMS, the values for $R^{bb}(VH)$ measured at the Tevatron should originate primarily from H_2 with $M_{H_2} \sim 135$–136 GeV;

This possibility is one of the main advantages of the present proposal.

However, the contribution of H_1 to the signal rate $R^{bb}(VH)$ obtained assuming $M_{H_{\rm SM}} \sim 135$ GeV can still be sizable, since the production cross section of H_1 is $\sim 30\%$ larger.

Assuming a mass resolution worse than 10 GeV, $R^{bb}_{135}(VH)$ in (16) would correspond to

$$R^{bb}_{\rm eff}(VH) \simeq R^{bb}_{2}(VH) + 1.3 \times R^{bb}_{1}(VH) \ . \qquad (18)$$

(In addition, the contribution from H_2 to the signal rate $R^{bb}_{125}(VH)$ should be as large as possible.)

NMSSM Model that does a good job

λ	0.617	$\mu_{\rm eff}$	143
κ	0.253	A_λ	164
$\tan\beta$	1.77	A_κ	337
M_{H_1}	125	M_{A_1}	95
M_{H_2}	136	M_{A_2}	282
M_{H_3}	289	$M_{H^\pm}$	272

Table 2: NMSSM-specific parameters and Higgs masses of a point with desired properties. (The dimensionful parameters are given in GeV.)

- The Higgs states are strongly mixed, both H_1 and H_2 having large SU(2) doublet and singlet components.

- H_1 has the smallest c_D component, which leads to an increase of the reduced branching fraction into $\gamma\gamma$ as discussed above.

  However, the partial width $\Gamma(H_1 \to \gamma\gamma)$ also receives an additional NMSSM-specific contribution of $\sim 20\%$ from higgsino-like charginos with

$m_{\tilde{\chi}_1^\pm} = 126$ GeV in the loop.

- The reduced branching fractions for the CP-even Higgs bosons are given in Table 3, and their signal rates relative to SM expectations in Table 4.

Higgs	$\frac{BR(H_i \to bb)}{BR(H_{\rm SM} \to bb)}$	$\frac{BR(H_i \to VV^{(*)})}{BR(H_{\rm SM} \to VV^{(*)})}$	$\frac{BR(H_i \to \gamma\gamma)}{BR(H_{\rm SM} \to \gamma\gamma)}$
H_1	0.73	1.52	2.21
H_2	1.46	0.62	0.54
H_3	43.45	0.08	1.37

Table 3: Reduced branching fractions for the three CP-even Higgs states. Note that we have $\frac{BR(H_i \to \tau\tau)}{BR(H_{\rm SM} \to \tau\tau)} \sim \frac{BR(H_i \to bb)}{BR(H_{\rm SM} \to bb)}$, and $\frac{BR(H_i \to WW^{(*)})}{BR(H_{\rm SM} \to WW^{(*)})} = \frac{BR(H_i \to ZZ^{(*)})}{BR(H_{\rm SM} \to ZZ^{(*)})} \equiv \frac{BR(H_i \to VV^{(*)})}{BR(H_{\rm SM} \to VV^{(*)})}$.

Higgs	$R^{\gamma\gamma}(ggF)$	$R^{\gamma\gamma}(VBF)$	$R^{VV^{(*)}}(ggF)$	$R^{VV^{(*)}}(VH)$	$R^{bb}(VH)$	$R^{\tau\tau}(ggF)$
H_1	1.30	1.09	0.90	0.75	0.36	0.42
H_2	0.16	0.27	0.18	0.31	0.74	0.43
H_3	0.58	0.01	0.04	0.004	0.23	19.6

Table 4: Reduced signal rates for the three CP-even Higgs states. Note that $R^{VV^{(*)}}(VBF) = R^{VV^{(*)}}(VH)$, and $R^{\tau\tau}(VBF) \sim R^{bb}(VH)$.

Do these signal rates have the desired properties listed earlier.

- We observe that $R_1^{\gamma\gamma}(ggF)$, $R_1^{ZZ^{(*)}}(ggF)$, $R_2^{\gamma\gamma}(ggF)$ and $R_2^{ZZ^{(*)}}(ggF)$ satisfy Eqs. (11), (12), (13) and (14), respectively.
- Note that $R_1^{\gamma\gamma}(VBF)$ is also enhanced, in agreement with the observations.
- In the $\tau\tau$ channel, $R_1^{\tau\tau}(VBF) = R_1^{bb}(VH)$ is indeed suppressed, as is $R_1^{\tau\tau}(ggF)$.
- $R_2^{\tau\tau}(VBF)$ is not enhanced but, as discussed earlier, $R_2^{\tau\tau}$ (like $R_2^{bb}(VH)$) can receive a considerable contribution from $R_1^{\tau\tau}$.

Indeed, for $R^{bb}_{\rm eff}(VH)$, defined by

$$R^{bb}_{\rm eff}(VH) \simeq R^{bb}_{2}(VH) + 1.3 \times R^{bb}_{1}(VH)\ , \tag{19}$$

we obtain $R^{bb}_{\rm eff}(VH) \sim 1.20$, with the dominant contribution from $R^{bb}_{2}(VH)$.

This value coincides with the large excess given in (16) (assuming a single Higgs state at 135 GeV) only within about two standard deviations, but at least exceeds the SM value.

- Finally, the signal rates in the $WW^{(*)}$ channel via VH are consistent with the present limits.

Semi-Constrained NMSSM GUT scenarios?

- One can find scenarios where H_1 and H_2 have masses of about 125 and 136 GeV, respectively.

- However, we did not find any points where the constraints (11) to (14) are all satisfied simultaneously —

at least one of the conditions on $R_1^{\gamma\gamma}(ggF)$, $R_2^{\gamma\gamma}(ggF)$ or $R_2^{ZZ^{(*)}}(ggF)$ has to be relaxed to find valid points.

For example, we can satisfy Eqs. (11), (12), (14) (and (15)), but then $R_2^{\gamma\gamma}(ggF)$ turns out too low, $R_2^{\gamma\gamma}(ggF) \lesssim 0.06$. Maybe a good thing in the end?

Or we can satisfy (12)–(15), but then $R_1^{\gamma\gamma}(ggF) \lesssim 1.3$. Moreover, $R_2^{bb}(VH)$ is never large, making it difficult to explain the Tevatron result in this channel.

Higgses at 98 GeV for LEP and 125 GeV for LHC:

(G. Belanger, U. Ellwanger, J. F. Gunion, Y. Jiang, S. Kraml and J. H. Schwarz. arXiv:1210.1976)

- We demonstrate that the two lightest CP-even Higgs bosons, h_1 and h_2, of the NMSSM could have properties such that the h_1 fits the LEP excess at ~ 98 GeV while the h_2 is reasonably consistent with the Higgs-like LHC signals at ~ 125 GeV, including in particular the larger-than-SM signal in the $\gamma\gamma$ channel.

  To describe the LEP and LHC data the h_1 must be largely singlet and the h_2 primarily doublet (mainly H_u for the scenarios we consider).

  An h_2 with $m_{h_2} \sim 125$ GeV and enhanced $\gamma\gamma$ rate is obtained, as in previous cases, at large λ and moderate $\tan\beta$.

- In order to display the ability of the NMSSM to simultaneously explain the LEP and LHC Higgs-like signals, we (once again) turn to NMSSM scenarios with semi-unified GUT scale soft-SUSY-breaking.

- All the accepted points correspond to scenarios that obey all experimental constraints (mass limits and flavor constraints as implemented in NMSSMTools, $\Omega h^2 < 0.136$ and 2011 XENON100 constraints on the spin-independent scattering cross section) except that the SUSY contribution to the anomalous magnetic moment of the muon, δa_μ, is too small to explain the discrepancy between the observed value of a_μ and the SM prediction.

- Fig. 15, the crucial plot, shows $R^{h_1}_{VBF}(bb)$ (which $= R^{h_1}_{Z^* \to Z h_1}(bb)$ as for LEP) versus $R^{h_2}_{gg}(\gamma\gamma)$ when $m_{h_1} \in [96, 100]$ GeV and $m_{h_2} \in [123, 128]$ GeV are imposed in addition to the above mentioned experimental constraints.[1]

  (In this and all subsequent plots, points with $\Omega h^2 < 0.094$ are represented by blue circles and points with $\Omega h^2 \in [0.094, 0.136]$ (the "WMAP window") are represented by orange diamonds.)

  Note that $R^{h_1}_{VBF}(bb)$ values are required to be smaller than 0.3 by virtue of the fact that the LEP constraint on the $e^+e^- \to Zb\bar{b}$ channel with $M_{b\bar{b}} \sim 98$ GeV is included in the NMSSMTools program.

[1] Here the Higgs mass windows are designed to allow for theoretical errors in the computation of the Higgs masses.

Those points with $R^{h_1}_{VBF}(bb)$ between about 0.1 and 0.25 would provide the best fit to the LEP excess.

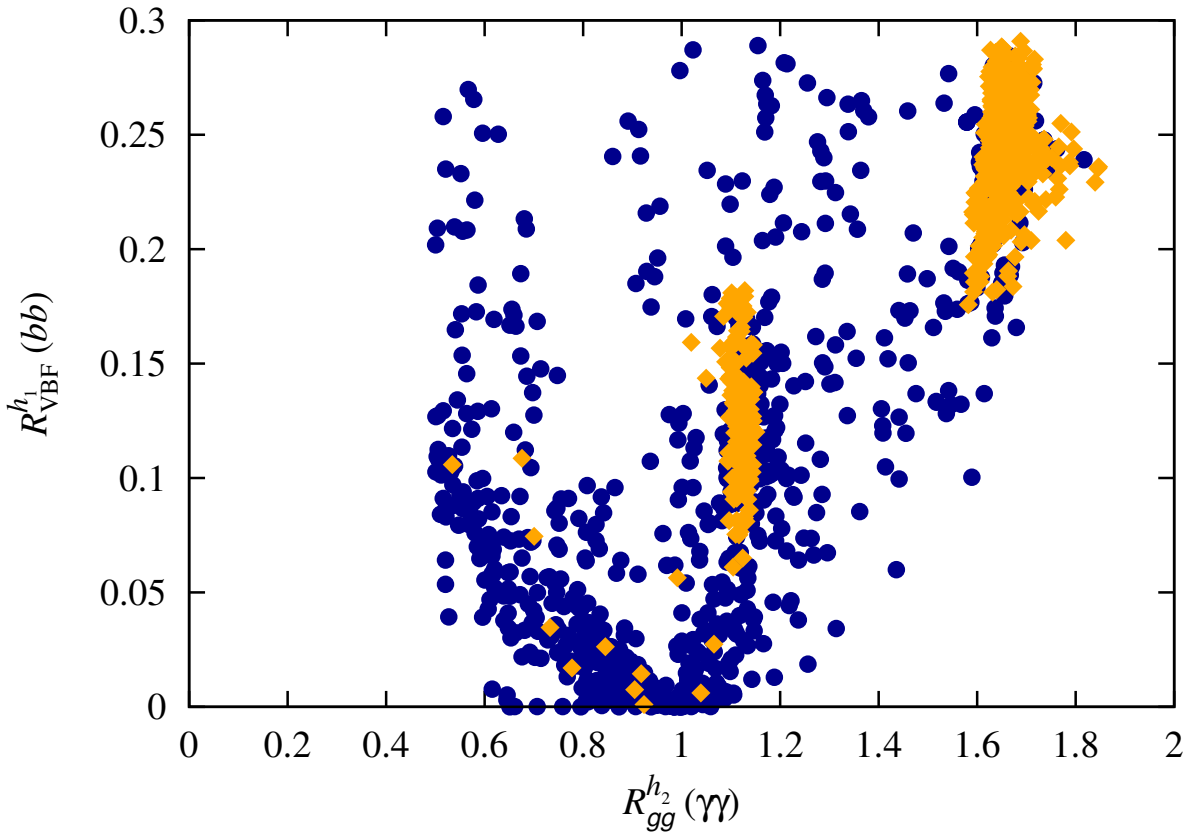

Figure 15: Signal strengths (relative to SM) $R^{h_1}_{VBF}(bb)$ versus $R^{h_2}_{gg}(\gamma\gamma)$ for $m_{h_1} \in [96, 100]$ GeV and $m_{h_2} \in [123, 128]$ GeV. In this and all subsequent plots, points with $\Omega h^2 < 0.094$ are represented by blue circles and points with $\Omega h^2 \in [0.094, 0.136]$ (the "WMAP window") are represented by orange diamonds.

To focus on scenarios for which the h_2 signal (at ~ 125 GeV) in $\gamma\gamma$ is enhanced and the LEP 98 GeV excess is well fit, in all the remaining plots we will impose the additional requirements: $R^{h_2}_{gg}(\gamma\gamma) > 1$ and $0.1 \leq R^{h_1}_{VBF}(bb) \leq 0.25$.

In the following, we will refer to these NMSSM scenarios as the "$98 + 125$ GeV Higgs scenarios" or "LEP-LHC scenarios".

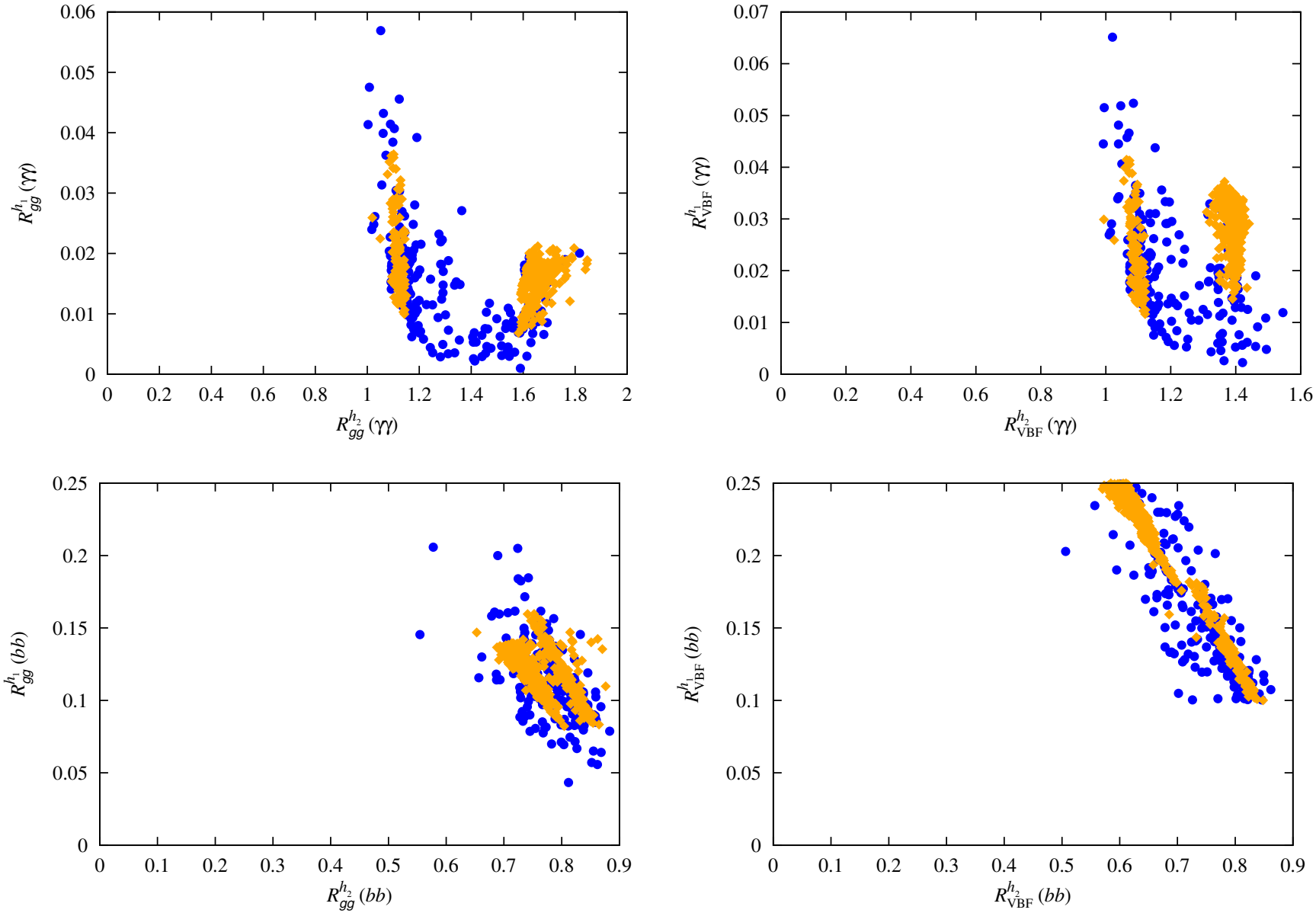

Figure 16: For $h = h_1$ and $h = h_2$, we plot (top) $R^h_{gg}(\gamma\gamma)$ and $R^h_{VBF}(\gamma\gamma)$ and (bottom) $R^h_{gg}(bb)$ and $R^h_{VBF}(bb)$ we show only points satisfying all the basic constraints as well as $m_{h_1} \in [96, 100]$ GeV, $m_{h_2} \in [123, 128]$ GeV, $R^{h_2}_{gg}(\gamma\gamma) > 1$ and $R^{h_1}_{VBF}(bb) \in [0.1, 0.25]$, *i.e.* the "$98 + 125$ GeV Higgs scenarios".

- In Fig. 16, the upper plots show that the h_2 can easily have an enhanced $\gamma\gamma$ signal for both gg and VBF production whereas the $\gamma\gamma$ signal arising from the h_1 for both production mechanisms is quite small and unlikely to be observable.

  Note the two different $R_{gg}^{h_2}(\gamma\gamma)$ regions with orange diamonds (for which Ωh^2 lies in the WMAP window), one with $R_{gg}^{h_2}(\gamma\gamma) \sim 1.1$ and the other with $R_{gg}^{h_2}(\gamma\gamma) \sim 1.6$.

  The first region corresponds to $m_{\tilde{\chi}_1^0} > 93$ GeV and $m_{\tilde{t}_1} > 1.8$ TeV while the second region corresponds to $m_{\tilde{\chi}_1^0} \sim 77$ GeV and $m_{\tilde{t}_1}$ between 197 GeV and 1 TeV.

  These same two regions emerge in many subsequent figures.

  If $R_{gg}^{h_2}(\gamma\gamma)$ ends up converging to a large value, then masses for all strongly interacting SUSY particles would be close to current limits if the present $m_{h_1} \sim 98$ GeV-$m_{h_2} \sim 125$ GeV scenario applies.

  The bottom row of the figure focuses on the $b\bar{b}$ final state. We observe the reduced $R_{gg}^{h_2}(bb)$ and $R_{VBF}^{h_2}(bb)$ values that are associated with reduced

$b\bar{b}$ width (relative to the SM) needed to have enhanced $R^{h_2}_{gg}(\gamma\gamma)$ and $R^{h_2}_{VBF}(\gamma\gamma)$.

Meanwhile, the $R^{h_1}_{gg}(bb)$ and $R^{h_1}_{VBF}(bb)$ values are such that the h_1 could not yet have been seen at the Tevatron or LHC. Sensitivity to $R^{h_1}_{gg}(bb)$ ($R^{h_1}_{VBF}(bb)$) values from 0.05 to 0.2 (0.1 to 0.25) will be needed at the LHC.

This compares to expected sensitivities after the $\sqrt{s} = 8$ TeV run in these channels to R values of at best 0.8.[2]

Statistically, a factor of 4 to 10 improvement requires integrated luminosity of order 16 to 100 times the current $L = 10$ fb^{-1}. Such large L values will only be achieved after the LHC is upgraded to 14 TeV.

Finally, note that for WMAP-window points the largest $R^{h_1}_{VBF}(bb)$ values occur for the light-$m_{\tilde{\chi}^0_1}$ point group described above for which supersymmetric particle masses are as small as possible.

[2] Here, we have used Fig. 12 of cmshiggs extrapolated to a Higgs mass near 98 GeV and assumed $L = 20$ fb^{-1} each for ATLAS and CMS.

- **Other NMSSM particles, properties and parameters, including $\widetilde{\chi}_1^0$ and $\widetilde{\chi}_1^\pm$ compositions**

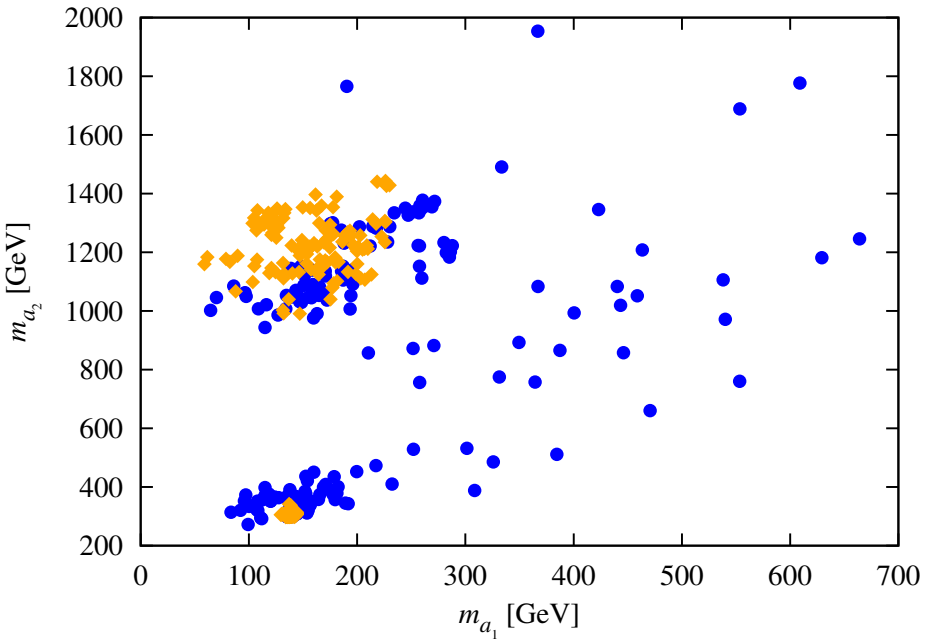

Figure 17: Scatter plot of m_{a_2} versus m_{a_1} for the 98+125 GeV scenario; note that $m_{a_2} \simeq m_{h_3} \simeq m_{H^\pm}$. Note that in this figure there is a dense region, located at $(m_{a_1}, m_{a_2}) \sim (130, 330)$ GeV, of strongly overlapping orange diamond points. These are the points associated with the low-$m_{\widetilde{\chi}_1^0}$ WMAP-window region of parameter space. Corresponding dense regions appear in other figures.

We note without a plot that the good Ωh^2 points all have $m_{\widetilde{\ell}_R}$, $m_{\widetilde{\nu}_\ell}$, $m_{\widetilde{\tau}_1}$ and $m_{\widetilde{\nu}_\tau}$ larger than 1.5 TeV.

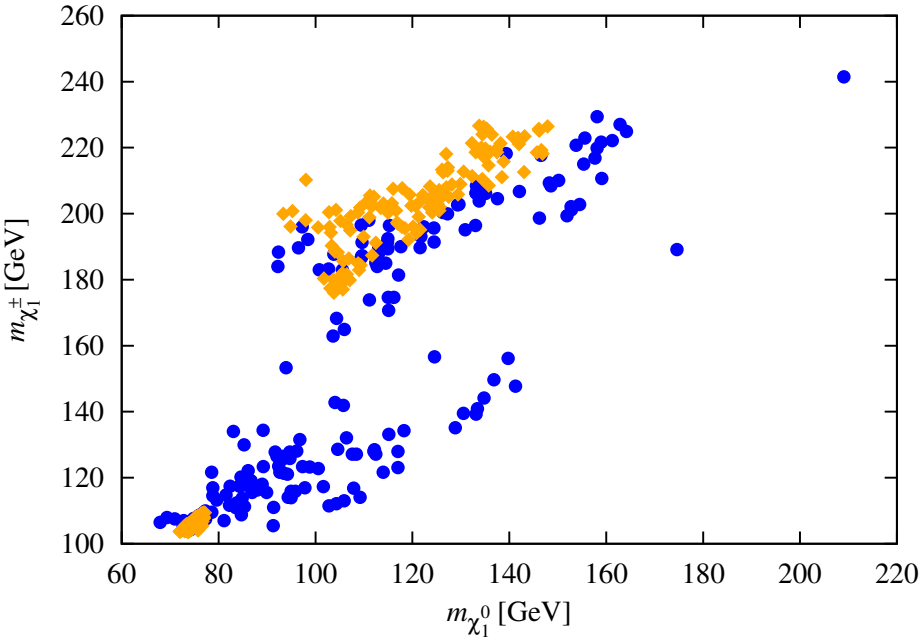

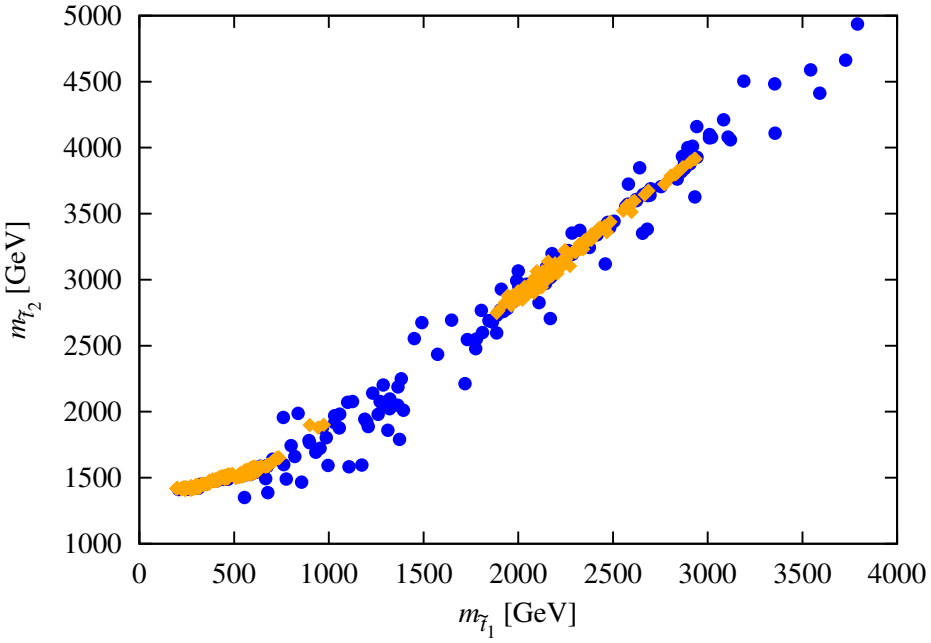

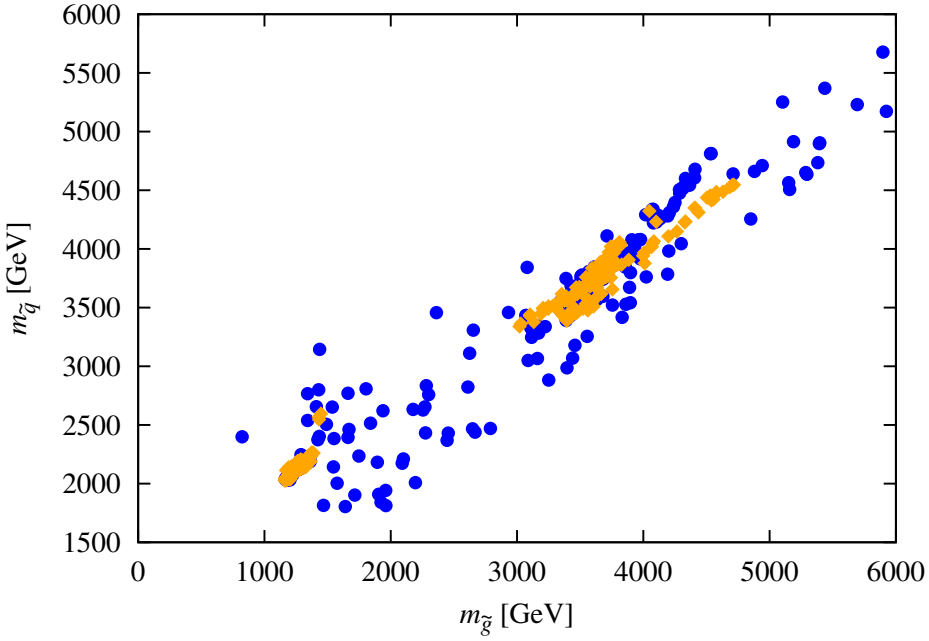

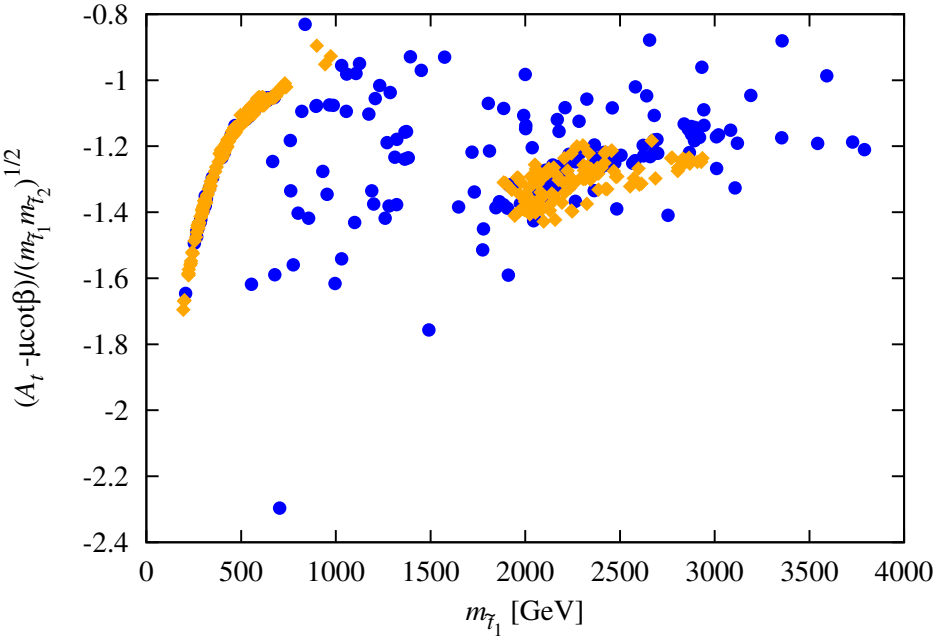

Figure 18: Plots showing $m_{\tilde{\chi}_1^0}$, $m_{\tilde{\chi}_1^\pm}$, $m_{\tilde{t}_1}$, $m_{\tilde{t}_2}$, $m_{\tilde{q}}$, $m_{\tilde{g}}$, and the mixing parameter $(A_t - \mu \cot\beta)/\sqrt{m_{\tilde{t}_1} m_{\tilde{t}_2}}$.

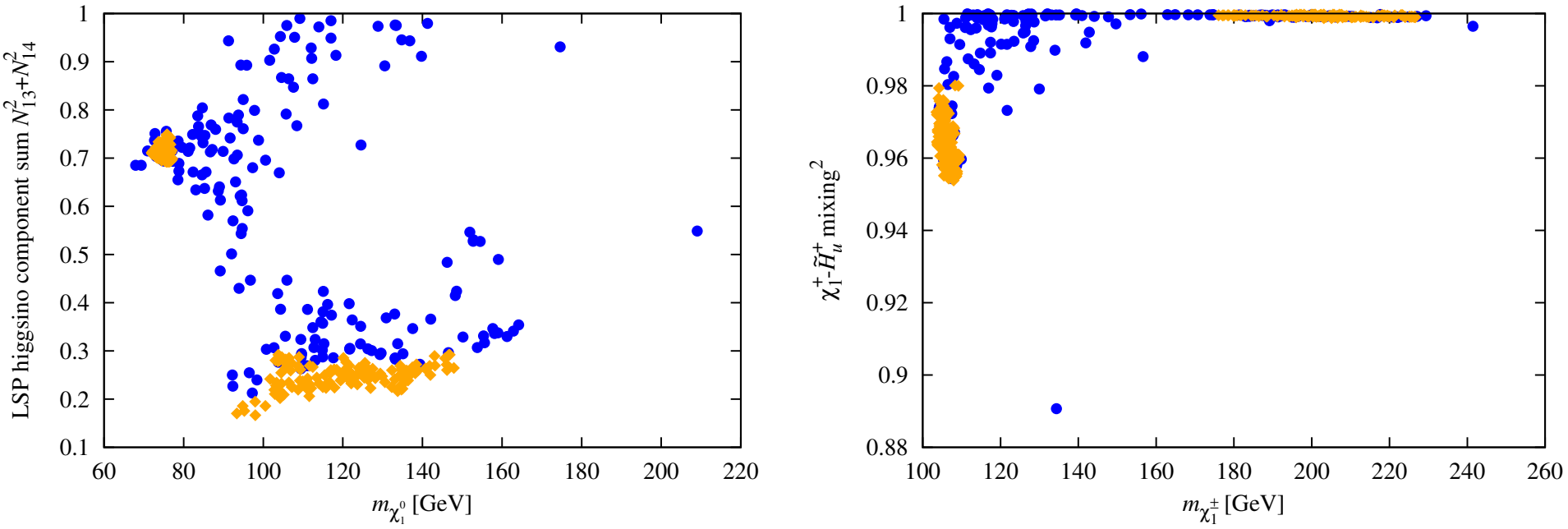

Figure 19: Neutralino and chargino compositions for the LEP–LHC scenarios.

Note that the $\widetilde{\chi}_1^0$ is very singlino in the low-$m_{\widetilde{\chi}_1^0}$ WMAP-window scenarios.

- **Input parameters**

The most important thing to note in the following figure is that the low-$m_{\widetilde{\chi}_1^0}$ WMAP-window scenarios have not only low $m_{\tilde{t}_1}$ but also low $\mu_{\rm eff}$, implying not much fine-tuning.

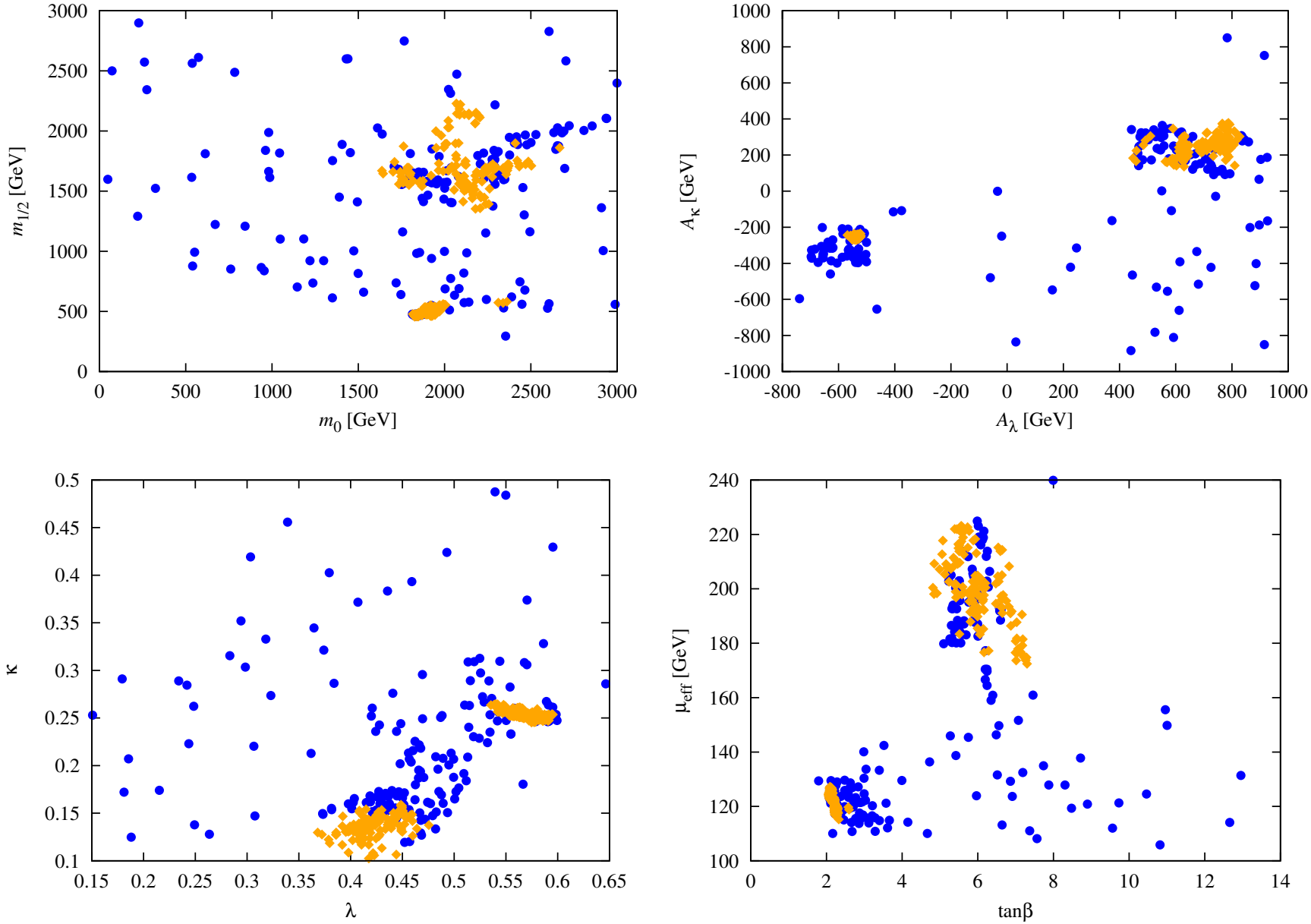

Figure 20: GUT scale and SUSY scale parameters leading to the LEP–LHC scenarios.

- **Dark Matter Issues**

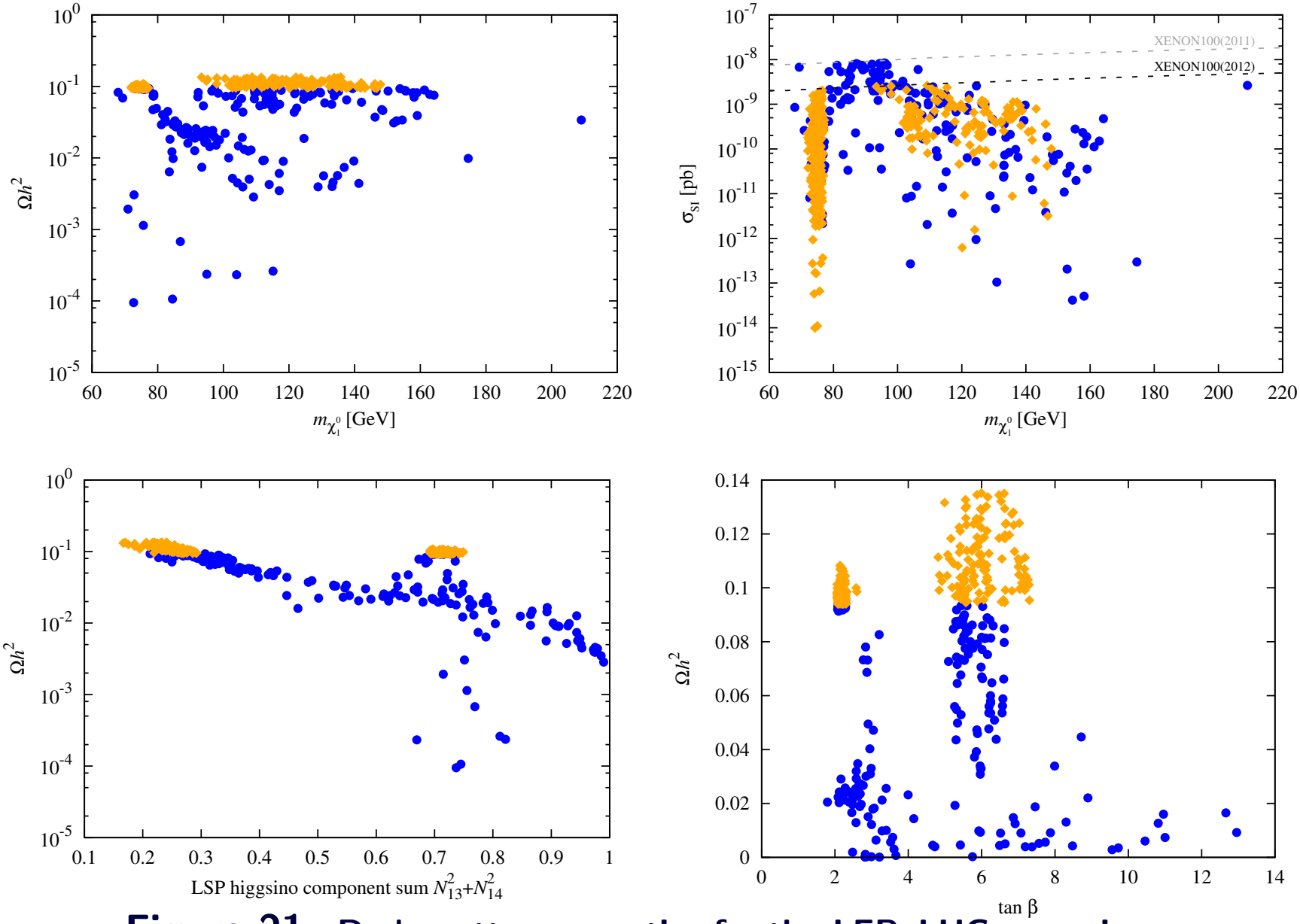

Figure 21: Dark matter properties for the LEP–LHC scenarios.

The composition of the $\widetilde{\chi}_1^0$ and the $\widetilde{\chi}_1^\pm$ are crucial when it comes to the relic density of the $\widetilde{\chi}_1^0$.

For those points in the WMAP window with low $m_{\widetilde{\chi}_1^0}$, the $\widetilde{\chi}_1^0$ can have a large Higgsino fraction since the $\widetilde{\chi}_1^0\widetilde{\chi}_1^0 \to W^+W^-$ annihilation mode (mainly via t-channel exchange of the light Higgsino-like — see second plot of Fig. 19 — chargino) is below threshold.

In contrast, the group of points with $m_{\widetilde{\chi}_1^0} > 93$ GeV can lie in the WMAP window only if the $\widetilde{\chi}_1^0$ does not have a large Higgsino fraction.

This division is clearly seen in Fig. 19. (We note that to a reasonable approximation the singlino fraction of the $\widetilde{\chi}_1^0$ is given by 1 minus the higgsino fraction plotted in the left-hand window of the figure.)

Dark matter (DM) properties for the surviving NMSSM parameter points are summarized in Fig. 21. Referring to the figure, we see a mixture of blue circle points (those with $\Omega h^2 < 0.094$) and orange diamond points (those with $0.094 \leq \Omega h^2 \leq 0.136$, *i.e.* in the WMAP window).

The main mechanism at work to make Ωh^2 too small for many points is

rapid $\widetilde{\chi}_1^0\widetilde{\chi}_1^0$ annihilation to W^+W^- due to a substantial higgsino component of the $\widetilde{\chi}_1^0$ (see third plot of Fig. 21). Indeed, the relic density of a higgsino LSP is typically of order $\Omega h^2 \approx 10^{-3} - 10^{-2}$.

As the higgsino component declines Ωh^2 increases and (except for the strongly overlapping points with $m_{\widetilde{\chi}_1^0} < m_W$, for which $\widetilde{\chi}_1^0\widetilde{\chi}_1^0 \to W^+W^-$ is below threshold) it is the points for which the LSP is dominantly singlino that have large enough Ωh^2 to fall in the WMAP window.

Also plotted in Fig. 21 is the spin-independent direct detection cross section, σ_{SI}, as a function of $m_{\widetilde{\chi}_1^0}$. We see that experiments probing the spin-independent cross section will reach sensitivities that will probe some of the predicted σ_{SI} values relatively soon, especially the $m_{\widetilde{\chi}_1^0} > 93$ GeV points that are in the WMAP window.

However, it is also noteworthy that the $m_{\widetilde{\chi}_1^0} \sim 75$ GeV WMAP-window points can have very small σ_{SI}.

The fourth plot of Fig. 21 and fifth plot of Fig 20 illustrate clearly the two categories of WMAP-window points.

The first category of points is that for which $m_{\widetilde{\chi}_1^0} > 93$ GeV, $\tan\beta \in [5, 7]$ and $\lambda \in [0.37, 0.48]$; the second category is that for which the $\widetilde{\chi}_1^0$ has low mass and large higgsino component with $\tan\beta \in [2, 2.6]$ and $\lambda \in [0.53, 0.6]$.

- **Direct Higgs production and decay at the LHC**

We have already noted in the discussion of Fig. 16 that gg and VBF production of the h_1 with $h_1 \to b\bar{b}$ provide event rates that might eventually be observable at the LHC once much higher integrated luminosity is attained. Other possibilities include production and decay of the a_1, a_2, and h_3.

Decay branching ratios and LHC cross sections in the gg fusion mode for a_2 and h_3 are shown in Fig. 22.

Since the a_1 is dominantly singlet in nature, its production rates at the LHC are rather small.

The a_2 is dominantly doublet and provides better discovery prospects.

- If $m_{a_2} > 2m_t$, the $t\bar{t}$ final state has $\sigma(gg \to a_2)\mathrm{BR}(a_2 \to t\bar{t}) > 0.01$ pb for $m_{a_2} < 550$ GeV, implying > 200 events for $L = 20$ fb^{-1}.
  A study is needed to determine if this would be observable in the presence of the $t\bar{t}$ continuum background.
  No doubt, efficient b tagging and reconstruction of the $t\bar{t}$ invariant mass in, say, the single lepton final state would be needed.
- For $m_{a_2} < 2m_t$, the $X = a_1 h_2$ final state with both a_1 and h_2 decaying to $b\bar{b}$ might be visible above backgrounds.
  However, a dedicated study of this particular decay mode is still lacking.

Similar remarks apply in the case of the h_3 where the possibly visible final states are $t\bar{t}$ for $m_{h_3} > 2m_t$ and $h_1 h_2$ for $m_{h_3} < 2m_t$.

For both the a_2 and h_3, $\sigma\mathrm{BR}(X)$ is substantial for $X = \widetilde{\chi}_1^0 \widetilde{\chi}_1^0$, but to isolate this invisible final state would require an additional photon or jet tag which would reduce the cross section from the level shown.

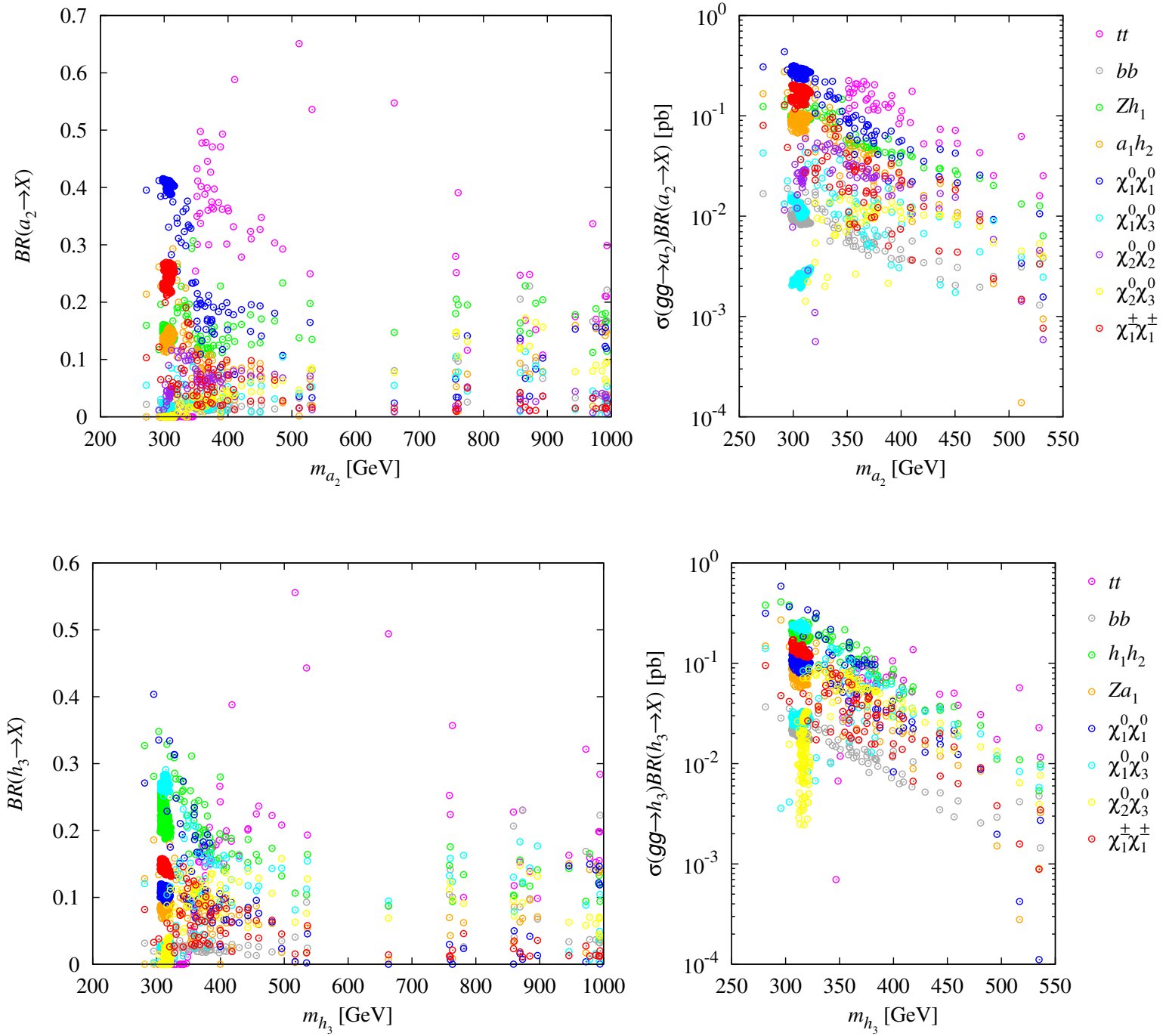

Figure 22: Decay branching ratios and LHC cross sections in the gg fusion mode (at $\sqrt{s} = 8$ TeV) for a_2 and h_3

Well, the story goes, with complicated decays of neutralinos and charginos to the various lighter Higgs bosons.

No time to go into it all here.

We do think this scenario is an intriguing one and hope experimentalists will educate themselves about some of its peculiarities.

It is possible, but far from guaranteed (in the low-$m_{\widetilde{\chi}_1^0}$ region), that σ_{SI} is large enough to be detectable soon.

Conclusions

- It seems likely that the Higgs responsible for EWSB has emerged.
- Perhaps, other Higgs-like objects are emerging.
- Survival of enhanced signals for one or more Higgs boson would be one of the most exciting outcomes of the current LHC run and would guarantee years of theoretical and experimental exploration of BSM models with elementary scalars.
- $>$SM signals would appear to guarantee the importance of a linear collider or LEP3 or muon collider in order to understand fully the responsible BSM physics.
- In any case, the current situation illusrates the fact that we must never assume we have uncovered all the Higgs.

Certainly, I will continue watching and waiting